Accurate and Efficient Multi-scale Flow Simulation using a Hybrid CFD-MD Approach ***Jeff: Another recommendation: Numerical and Computational Investigations on Hybrid CFD-MD Simulations

Soon-Heum Ko[a], Nayong Kim[b], Dimitris Nikitopoulos[d], Dorel Moldovan[d], Shantenu Jha[b,c,*]

[a] *National Supercomputing Centre, Linköping University, Linköping, SE-581 83, Sweden*
[b] *Center for Computation & Technology, Louisiana State University, Baton Rouge, LA 70803, USA*
[c] *Department of Computer Science, Louisiana State University, Baton Rouge, LA 70803, USA*
[d] *Department of Mechanical Engineering, Louisiana State University, Baton Rouge, LA 70803, USA*

Abstract

We investigate numerical and computational issues associated with hybrid computational fluid dynamics (CFD) - molecular dynamics (MD) simulation methodologies. Our current hybrid CFD-MD simulation framework is based on reliable CFD and MD codes linked together through hybrid interfaces that are often based on constrained Lagrangian dynamics for data exchange between continuum and MD regions. We argue that (1) the statistical error associated with the sampled average of the molecular solution, and (2) hybrid boundary conditions via an extrapolation methodology, may lead to non-negligible spatial and temporal inaccuracies of the hybrid solution. Hence, in this study we propose two strategies for minimizing the statistical noise inherent in the MD solution: (1) optimization of coupling parameters through the molecular dynamic simulation of a stationary flow field, and (2) averaging over multiple independent replicas of the simulation

*Corresponding author, (Tel)+1-225-578-XXXX; (FAX)+1-225-578-XXXX
Email addresses: sko@nsc.liu.se (Soon-Heum Ko), nykim@cct.lsu.edu (Nayong Kim), meniki@me.lsu.edu (Dimitris Nikitopoulos), moldovan@me.lsu.edu (Dorel Moldovan), sjha@cct.lsu.edu (Shantenu Jha)

system. In addition, we introduce a new temporal coupling scheme based on a 'prediction-correction' approach together with interpolation in time, which provides a more time-accurate hybrid constraint/boundary condition. With respect to computational performance, co-scheduling and load-balancing of logically distributed tasks are two important considerations in CFD-MD coupled simulations. We employ a BigJob computational framework, similar to a Pilot-job, and incorporate a load-balancing function for the computing efficiency of coupled simulation. The optimized hybrid framework is applied to solving two classical flow problems under Stokes (no interial effects) conditions. One is the impulsively started Couette flow, and the other is an oscillating boundary Stokes flow, which is induced by the periodic motion of one flat plate in the channel system. We emphasize that (1) the determination of coupling parameters through the molecular dynamic simulation of a stationary flow and the averaging of multiple independent replicas contribute much on suppressing the statistical noise in relatively low-speed flow fields of O(10) m/s velocity, (2) the accuracy of unsteady flow solution is increased by applying a 'prediction-correction' temporal coupling scheme, and (3) efficient coupled simulation is conducted by employing a BigJob computational framework along with the load-balancing capability.

Keywords: Hybrid computational fluid dynamics - particle dynamics approach, Constrained Lagrangian dynamics, Temporal coupling scheme, Simple API for Grid Applications, BigJob framework

---

1. Introduction and Motivation

A hybrid continuum dynamics - particle dynamics approach is an approach capable of describing accurately a flow at both macroscopic and molecular scales. In this approach the system is divided into two domains. A continuum formulation is used appropriately for one domain and a particle formulation (e.g. molecular dynamics) is applied to the other. Naturally the particle domain is more appropriate for material interfaces (e.g. fluid/solid or fluid/fluid) where molecular effects are more likely to be important. On the other hand, the continuum approach provides a better computational efficiency than particle dynamics with acceptable accuracy in solving the bulk flow field. In the hybrid approach the two domains are coupled through an overlap region/interface in which both formulations are valid. The overlap domain enables the exchange of conservative flow properties between

the continuum and particle ones so that the respective solutions are mutually consistent. The information from the continuum domain is passed to the particle domain by imposing additional numerical modeling to preserve higher degree-of-freedom on the particle motion, while the particle domain provides boundary conditions to the continuum domain obtained through time and spatial averaging of the relevant variable.

Despite the recent developments reported in the literature, most of which tested against small idealized pure atomistic flow simulations for comparison, there are still methodological and implementation issues that need refinement, testing and validation. In this section, we will give a brief account of the numerical and computational issues associated with some of the previous hybrid CFD-MD implementations and outline our approach to address them effectively.

1.1. Previous Hybrid CFD-MD Implementations

Hybrid CFD-MD simulations have utilized constrained Lagrangian dynamics [1–7], the Schwarz method [8–12], or a direct flux exchange [13–18] method, depending on the methodology used to impose the solution matching in the overlap region/interface and the nature of the variables that exchange information in this region. O'Connell and Thompson [1] were among the first to implement a hybrid CFD-MD simulation approach by introducing the overlap region that allows matching of the solutions from the two domains to relax smoothly before they are coupled together. Namely, they employed a relaxation method according to which the average MD velocity in an overlap region is forced to follow the continuum solution in the same region. In their implementation they use constrained Lagrangian dynamics according to which the particles are accelerated/decelerated in the overlap region so that on average they follow the continuum velocity. The drawback of their implementation is the arbitrariness of the relaxation rate and the lack of particle exchange (particle flux) between the two domains. This approach is refined by Nie *et al.* [2] who imposed the spatial coupling between continuum equations and molecular dynamics through constrained dynamics implemented in the overlap region. The implementation of Nie at al. can also account for the presence of mass flux across the MD-continuum interface implemented via a particle exchange algorithm. The methodology has been applied to a variety of flow problems such as the impulsively started Couette flow [1], channel flow with rough walls [2], cavity flow [3], Poiseuille flow [6] and the oscillating boundary problem [5, 7]. The use of direct constrained

dynamics equation makes this approach easy to implement and computationally efficient. However, the absence of energy exchange modeling limits the applications to isothermal systems. [13]

To alleviate some of these shortcomings, Hadjiconstantinou *et al.* [8–10] have introduced a new hybrid simulation methodology based on the Schwarz method. In this approach, the continuum solution is used to generate the solution in the particle domain in which the particle velocities are drawn from a Maxwellian distribution such that the mean velocity and the corresponding standard deviation are determined by the continuum solution and temperature [9]. This approach later was expanded to non-periodic boundary condition problems by Werder *et al.* [11], who also expanded and refined the previous boundary force models [1, 2, 13, 15] so as to minimize local disturbance. An alternating Schwarz approach has been applied to the moving contact line problem [9], Poiseuille flow [10], flow around the cylinder [11], and Couette flow of water [12]. The characteristics of decoupled physical time-scales between two domains makes this approach appealing when solving the flow field in problems in which hydrodynamic characteristic time scale is much larger than molecular dynamic time scale, i.e., micrometer system size. [9]

In order to be able to simulate isothermal compressible flow, Flekkϕy *et al.* [13] introduced a new hybrid method based on continuity of mass and momentum fluxes across the MD-continuum interface, which later included energy transfer [14, 15]. Further developments were implemented by Delgado-Buscalioni and Coveney [16] by introducing a particle insertion algorithm which satisfies the continuity of the mass flux along the interface while preserving the mean potential energy of the system. This approach has been applied to the study of Couette and Poiseulle flow [13], transversal wave [15], and oscillating boundary problem [17]. According to Flekkϕy *et al.* [13], flux exchange directly implies adherence to the relevant conservation laws without the use of constitutive relations and equations of state (to maintain the conservation laws). However, it is pointed out that the sampling time to measure fluxes within acceptable statistical error is orders of magnitude larger than the time to measure densities [10].

1.2. Numerical and Computational Issues Associated with Hybrid CFD-MD Methodologies

This unrealistic flow condition is unavoidable according to the mathematical analyses on the strength of statistical error (in other words, a signal-to-

noise ratio) [10, 17]. Sampling duration to maintain the same statistical error is proportional to $1/{u_\infty}^2$ and $1/N_0$, where u_∞ is a free stream condition and N_0 denotes the number of particles contained in sampling layer. So, reducing the free stream velocity by 1/10 requires 100 times more particles to be averaged to maintain the same statistical error. (Increasing the sampling duration is avoided because it can fail to describe the unsteady flow evolution.) This necessitates a different design of a hybrid simulation framework.

is adopted as the instantaneous solution at continuum domain. As the remedy, Liu *et al.* [7] proposed a multi-timescale algorithm by considering quasi-steadiness and Wang and He [5] proposed passing the extrapolated continuum solution to the MD solver. However, a multi-timescale algorithm is only valid if the period of unsteady phenomenon is sufficiently longer than sampling duration and particles lose their history during the re-initialization process in between sampling interval: Approach by Wang and He is a possible approach to mitigate the time-lagging effect though not in perfection.

Despite the recent developments and obvious advantages of a hybrid approach for flowing systems with scales straddling molecular to macroscopic (continuum) magnitudes over pure CFD or MD, a number of numerical and computational difficulties prevent this technique from being widely used. One of the difficulties is the lack of a clear methodology for defining an optimized set of parameters related to the coupling of the continuum and molecular domains. In general the flow solution obtained by a direct hybrid approach suffers from the existence of significant noise in the spatially averaged particle velocity mainly due to the inherent statistical fluctuations in the molecular description. Therefore, coupling parameters such as the size of the overlap domain and its position, the width of various layers and bins in the overlap region, and the sampling conditions, should be appropriately determined a priori in order to achieve more accurate numerical solutions. Many of these coupling parameters are problem dependent and this complicates the problem even further. Given the stochastic nature of the noise characterized by the mean velocities in the molecular domain of the coupling region, the characteristics of fluid and solid elements, as well as the geometric characteristics of material (e.g. fluid/solid) interfaces, it is difficult to develop a mathematical model capable of predicting the optimum coupling parameters. There have been some attempts to mittigate the inaccuracies associated with inherent statistical fluctuations by introduction of certain numerical damping terms in the equations of motion of the atoms in the overlap region [1, 4] or by defining a specific dynamic parameter to controlling the coupling in-

tensity [5], but all of these eventually lead to some violation of energy and momentum conservation.

Important issues remain to be addressed in the hybrid implementations for studying flow physics at moderate or low velocity conditions. So far, most of the reported studies have been confined to relatively high-speed flow conditions, of the order of 100 m/s, in nanoscale systems; flow conditions chosen mainly to obtain a high speed shear rate in the overlapping region and, more importantly, to reduce the relative stochastic thermal noise associated with the velocity flow field. [6] According to the mathematical models [10, 17] the noise level characterizing the average velocity in the coupling region in a hybrid CFD-MD implementation is proportional to $1/{u_\infty}^2$, where the u_∞ is the far field stream velocity, and to $1/N_0$, where N_0 denotes the number of particles contained in the sampling layer. Therefore, by reducing the free stream velocity by, say, 10 times, in order the maintain the same noise level (same statistical error) would require the increase of the number of particles in the averaging bins by 100 times, assuming that the sampling duration is maintained constant. In general the increase of the sampling duration beyond the limits imposed by the physical time-scales of a given unsteady flow problem is to be avoided because it leads to unphysical effects.

The accuracy of temporal coupling schemes is of great importance when solving unsteady problems. In general the temporal coupling scheme encompasses the timing of data exchange between the CFD and MD solvers, so as to synchronize both solutions at the same physical time instant. In this one has to keep in mind that the interpretation of the term "instantaneous" regarding values of variables differs between the continuum and molecular formulations. The time-coupling models are inherently affected by time-lagging. This is more pronounced when backward-averaged molecular dynamic properties are in general communicated as instantaneous properties to the continuum domain. To address this shortcoming, Liu *et al.* [7] proposed a multi-timescale algorithm by considering quasi-steadiness and Wang and He [5] proposed passing the extrapolated continuum solution to the MD solver. Despite their success there are, however, serious limitations with these approaches as a multi-timescale algorithm is only valid if the characteristic time of the unsteady phenomenon is substantially longer than the integration (averaging) time of the MD solutions. This is also a prerequisite for the particle (MD) solution to be able to equilibrate subject to the constraint passed on from the continuum solution from one continuum time instant to another. The approach by Wang and He may therefore be a good compromise that

may mitigate some of the time-lagging effects.

In addition to the above mentioned issues, there are computational challenges related to the integration of multiple application domains into a single problem set. Due to their very different computational kernels (e.g. one mesh-based, the other an unstructured particle-based), it is difficult to incorporate distinct CFD and MD codes under the umbrella of a single tightly-coupled application (i.e. unifying two application codes to share a single MPI communicator). One possible alternative can be to implement a coupling interface into one of the individual codes and design it such that this assumes control of the two separate codes as a virtually unified simulation package. This heterogeneous implementation raises additional computational challenges. For example, in the parallel execution of such a simulation package, on conventional production systems with batch queues, it cannot be guaranteed that two separate jobs will execute concurrently. Considering the computational characteristics of the current application, where the CFD and MD codes conduct frequent data exchange, the first job that completes a task will inevitably experience the idle waiting for its counterpart to finish its sequenced task without the explicit support for co-scheduling. Another important challenge is the need for efficient load-balancing which takes into account the individual application's performance. Even if the two simulations could run concurrently, without explicit load-management/balancing support, there is likely to be inefficient utilization of computing resources due to load imbalance. As the performance of each simulation component changes with computing resource and problem size, re-adjustment of allocated resources to each task according to their performance is required during the hybrid simulation.

1.3. Objectives and Outline of the Paper

The focus of this paper is to investigate numerical issues associated with the implementation of a typical hybrid CFD-MD methodology applied to investigate the flow in a nano/micro-fluidic system as well as with designing and developing of an efficient runtime framework for coupled multi-scale simulations. We present our implementation of a 'generic' hybrid CFD-MD interface which can be easily put together from various 'off the shelf' incompressible CFD and MD packages, as well as our model of a 'portable' framework that can be ported easily on most present day computer architectures.

We present the development of our hybrid simulation framework, based on constrained Lagrangian dynamics, and apply it to two prototype classical flow problems: the impulsively started Couette flow and an oscillating boundary Stokes flow. From the pure MD solution on zero-velocity flow field, we elaborate on our strategy for determining the optimized set of coupling parameters that minimize the level of the statistical noise characterizing the flow field obtained by the hybrid solver. In addition we extend our investigation into the moderate-speed flow regime (flow velocities of the order of 10 m/s), which is challenging and novel. The inherent large fluctuations of the solution in the overlap region associated with relatively low flow speed are reduced by a multiple replica averaging methodology. For the oscillating boundary Stokes flow simulation, we demonstrate a novel temporal coupling scheme, called 'rrediction-correction approach' which provides improved accuracy by eliminating the overshoot/undershoot phenomena and diminishes the time-lagging pattern.

In terms of computational science, our study introduces a novel approach to coupled multi-physics simulations by utilizing the virtually unified simulation package, called "Pilot-Job". We argue that using the Pilot-Job approach has distinct advantages, such as: (i) elimination of the need for a co-scheduler while preserving performance, and (ii) enables dynamic resource allocation, which in turn is important for load-balancing across coupled simulations.

The paper is organized as follows. In Section 2 we give a brief description of the fundamental equations describing the CFD and MD formulations as well as details of the hybrid CFD-MD coupling scheme and its implementation. Technical details related to the implementation of an efficient CFD-MD simulation framework are presented in Section 3. In Section 4, we present the solutions to the two prototype problems (impulsively started Couette flow and oscillating boundary Stokes problem) obtained with our hybrid methodology. The performance and the optimization issues related to the solutions of the two test problems are described in Section 5. Recommendation for future work and conclusions are presented in Sections 6 and 7.

2. Fundamentals of the Hybrid Coupled CFD-MD Simulation Toolkit

The accuracy of a hybrid CFD-MD solution is governed by the underlying numerical schemes in individual solver as well as hybrid schemes implemented. We explain the features of baseline solvers and the structure of hybrid interface in this section. We also investigate additional numerical

treatments to improve the accuracy of hybrid CFD-MD simulations in various types of fluid systems. ***NKim:
========== Modified version from ME ==========
The accuracy of a hybrid CFD-MD solution is governed by the underlying numerical schemes of the individual continuum and particle solvers as well as the coupling scheme. This section details and explains the features of baseline solvers and the structure of the hybrid coupling interface. Additional numerical treatments to improve the accuracy of hybrid CFD-MD simulations in various types of fluid systems are also addressed.

2.1. Overview of the Continuum-Molecular Coupled Approach

The hybrid CFD-MD approach stands on the proposition that the molecular dynamic simulation produces more accurate solution than the continuum model and a more efficient continuum solver provides the boundary condition to particle domain without restricting the high degree-of-freedom of atomistic motion. So, the region which contains a strong flow gradient is resolved by a molecular dynamic simulation and moderate flow in macroscopic scale is captured by the continuum dynamics. Also, these problem domains overlap each other in the middle to exchange the individual information.

A detailed structure of the fluid domain for constrained Lagrangian dynamics models is described in Fig. 1. CFD approach solves the external zones with the moderate flow velocity and MD analyzes the complex microscopic flow feature near the stationary obstacle or in the low-speed region. Hybrid region is placed sufficiently far from the solid obstacle to prevent the direct influence of strong fluctuation near the solid-fluid interface. Also, this region is designed sufficiently large to contain five layers with enough spacing.

Roles of these layers in hybrid region are as follows. From the bottom, we have the *particle-to-continuum* and *continuum-to-particle* (denoted as 'MDtoCFD' and 'CFDtoMD', respectively) boundary zones for CFD and MD simulations, and have additional zone to exert external force. These three interesting zones are isolated by the buffer in between. Particles' properties spatially located in the MDtoCFD boundary layer are averaged over a finite time (called 'sampling duration') and they are transferred to continuum solver at constant period (called 'sampling interval'). The height of each layer is the same as the CFD cell height and averaged conservative properties in two consecutive layers are passed to continuum domain to be directly imposed as the viscous boundary condition on the Navier-Stokes

solver with collocated data structure. Next, the hybrid MD boundary zone is placed in the middle. In this region, the instantaneous continuum solution is transferred to MD code. Particles in this layer are guided to eventually follow this macroscopic flow velocity, by solving a constrained Lagrangian dynamics equation. The strong point of this equation is that, molecules are led to follow the macroscopic flow property, while preserving their degree-of-freedom of translational motion. In the uppermost layer, the external force is exerted on particles to conserve system's statistical ensembles. This force function is designed not too strong to influence the motion of particles in the domain of interest nor not too weak to have particles drifting away. Finally, buffer layer is positioned in between each layer. This layer is set up to be bigger than the length scale of interacting particles (cutoff radius), not to have a solution in one layer being directly interfered by another solution.

***NKim:

========== Modified version from ME ==========

The hybrid CFD-MD approach stands on the proposition that (a) the molecular dynamic simulation produces a more physically accurate solution in its domain than the continuum model would, (b) a faster and more efficient CFD solver provides a physically accurate solution in the continuum domain, which would be prohibitive if a particle representation were to be used, and (c) the two solutions can be reconciled by the mutual exchange of information, the continuum solution providing the constraint to the particle solution while the latter providing a boundary condition to the former. So, the region within which molecular-level physics are important (e.g. a material interface) is treated and resolved by a molecular dynamic simulation, while the region within which the continuum-level physics adequately represent the transport processes on a macroscopic scale is treated and resolved by the continuum CFD. The continuum and particle (molecular) domains overlap, in this approach, so as to exchange information for the coupling. Obviously, the overlap domain must be one where both treatments/formulations are valid. A detailed structure of the various domains associated with the hybrid CFD/MD methodology is described in Fig. 1. CFD solves the continuum equations in the ?ure CFD Region? while MD resolves the microscopic (particle) flow in the ?ure MD region? The latter is a solid stationary wall for the two test problems examined herein. The hybrid (overlap) region is placed sufficiently far from the solid wall to prevent direct constraint of the molecular-level physics in the proximity of the solid-fluid interface. This overlap region is designed sufficiently large to contain five individual layers

of sufficient width for the purpose of their existence. The widths of these layers are of course problem dependent. Their roles in the hybrid region are as follows. One layer (the bottom one in Fig. 1-left) provides information from the particle (MD) domain to the continuum one (denoted as ?DtoCFD?. A second layer (the third one from the bottom in Fig. 1-left) provides information from the continuum domain to the particle one (denoted as ?FDtoMD?. A third layer (the top one in Fig. 1-left) applies a fictitious external force which prevents particles from escaping from the hybrid domain. These three ?ctive?layers are separated by buffer layers, which are placed so as to ensure smooth transitions and that there is no direct correlation between the ?ctive?layers. Properties (e.g. velocity) of particles spatially located in the MDtoCFD layer are ensemble-averaged over all the particles in the layer and also averaged over a finite time (?ampling duration?. The average value is communicated to the continuum solver periodically with a fixed period (?ampling interval?. The height of each layer is the same as the CFD cell height and averaged conservative properties in two consecutive layers are passed to continuum domain to be directly imposed as the viscous boundary condition on the Navier-Stokes solver with collocated data structure. The CFDtoMD layer imposes the instantaneous values of properties, velocity in this case, resulting from the continuum solver. This is done via and appropriate constraint to the MD particle-based conservation of momentum on every single particle (constrained dynamics) in the CFDtoMD layer. Thus, particles in this layer are constrained to attain the macroscopic flow property (velocity in this case) on average, while preserving their degree-of-freedom of translational motion. In the uppermost layer, a fictitious external force is exerted on particles to prevent them from escaping the particle domain. This force function is designed to be short-range so as not to be strong enough to influence the motion of the particles past the buffer layer in the CFDtoMD domain. The force stiffens as the particles approach the location where the force becomes infinite in a way that minimizes reflections while preventing the particles from drifting out of the particle domain. The buffer layers existing in between each ?ctive?layer are set up to be wider than the interaction length scale of the particles (cutoff radius), in order to prevent direct interaction between particles in neighboring ?ctive?layers.

***Jeff: It would be better to explain a little more detail on last sentence. Let's say the buffer between CFDtoMD and MDtoCFD boundary is smaller than cutoff length. Then, a solution at CFDtoMD (constrained MD)

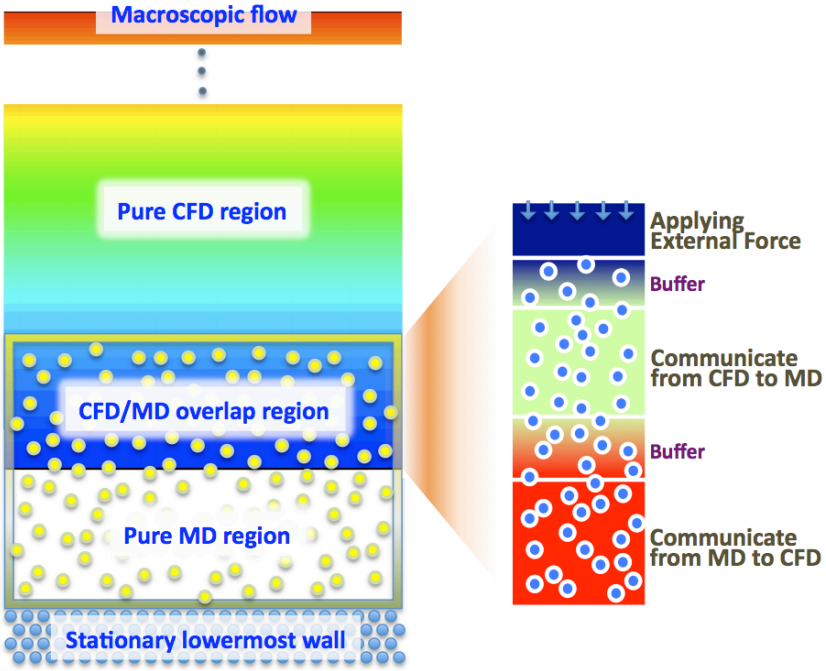

Figure 1: Schematic Diagram of the Hybrid Domain with Detailed View of Overlapping Zone; Overall continuum/atomistic computational domain including overlap region is shown on left figure. Detailed layer by layer explanation of overlapping region is indicated by right figure. ***NKim: Modified version from ME : Schematic diagram of the overall continuum/atomistic and hybrid computational domains for the chosen test problems (left) including a detailed view of the overlapping zone (right)

directly affects the motion of particles at MDtoCFD. And this is used for CFD boundary condition. This results that, CFD solution at CFDtoMD is the result of flow variation in MDtoCFD boundary, which in turn is directly affected by the CFDtoMD solution. Thus, solution at CFDtoMD becomes the boundary condition of CFD domain.

2.2. Governing Equations and Numerical Schemes

2.2.1. Continuum Incompressible Flow Formulation (CFD)

The current in-house continuum hydrodynamics code solves the unsteady incompressible Navier-Stokes equations to demonstrate the isothermal nano-scale flow field: ***NKim:
========== Modified version from ME ==========
The current in-house continuum hydrodynamics code solves the unsteady

incompressible Navier-Stokes equations:

$$\frac{\partial u_i}{\partial x_i} = 0 \tag{1}$$

$$\frac{\partial u_i}{\partial t} + \frac{\partial}{\partial x_j}(u_i u_j) = -\frac{\partial p}{\partial x_i} + \nu \frac{\partial^2 u_i}{\partial x_j \partial x_j}$$

where ν is the kinematic viscosity.

In this work, the pseudo-compressibility method [19] is adopted to form a hyperbolic system of equations which can be marched in pseudo-time. A time derivative of pressure is added to the continuity equation resulting in

$$\frac{\partial (p/\rho)}{\partial \tau} = -\beta \frac{\partial u_i}{\partial x_i} \tag{2}$$

where β denotes a pseudo-compressibility parameter, currently set up to 2.5.

For time-accurate unsteady simulation, a dual time stepping method is adopted and it is combined with the LU-SGS (Lower-Upper Symmetric Gauss-Seidel) scheme [20] for the implicit time integration. The inviscid fluxes are upwind-differenced using Osher's flux-difference splitting scheme [21]. For higher-order spatial accuracy, the MUSCL (Monotone Upstream-centered Schemes for Conservation Laws) [22] approach is used on an inviscid flux calculation. Viscous fluxes are calculated using conventional second-order central differencing.

2.2.2. Molecular-Level Formulation (MD)

In MD, an initial velocity is assigned to each atom, and Newton's laws are employed at the atomic level to propagate the system's motion through time evolution. To calculate pairwise interactions of particles in the system, the most commonly used Lennard-Jones (12-6) potential interaction model is employed and is define as: ***NKim:
========== Modified version from ME ==========
In MD, an initial velocity is assigned to each atom, and Newton? conservation of momentum is employed at the atomic level to propagate the system? motion through time evolution. In this work the most commonly used Lennard-Jones (12-6) intermolecular force potential model is employed

to calculate pair-wise interactions of particles in the system, and is defined as:

$$u(|r_i - r_j|) = 4\epsilon_{ij}[(\frac{\sigma_{ij}}{r_{ij}})^{12} - (\frac{\sigma_{ij}}{r_{ij}})^{6}] \tag{3}$$

where ϵ_{ij} and σ_{ij} denote the pairwise potential well depth and the atom size parameter respectively, and r_{ij} is the distance between the particle i and j. The term $1/r_{ij}^{12}$ dominating at short range distance repulsive behavior based on the Pauli principle to avoid overlapping the electronic clouds when particles are brought very close to each other. The term $1/r_{ij}^{6}$ dominates at long range attractive forces by van der Waals dispersion forces. The cut-off distance σ_c is introduced here to reduce the computational cost and is set to be 2.2σ [23].

The time integration algorithm is required to integrate the equation of motion of the interacting particles and computing molecular trajectories, one of most common velocity Verlet algorithm is employed to compute the simulation.

In this work, the MD simulations were performed by using the modified version of Large Atomic Molecular Massively Parallel Simulator(LAMMPS). It is the classical molecular dynamics open-source code written in C++ and developed by Sandia National Labs. [24]

***NKim:

========== Modified version from ME ==========

where ϵ_{ij} and σ_{ij} denote the pair-wise potential well depth and the atom size parameter respectively, and rij is the distance between the particle i and j . The repulsive term 1 /rij12 dominating at short rij distance is based on the Pauli principle to avoid overlapping the electronic clouds when particles are very close to each other. The attractive term 1/rij6 dominates at long range representing Van der Waals dispersion forces. A cut-off distance σ_c is introduced here to reduce the computational cost and is set to be 2.2σ [28]. Namely when rij exceeds the cutoff the intermolecular force is set to zero without being calculated. The most common velocity Verlet algorithm is employed for time integration of the equations of motion of the interacting particles and to compute molecular trajectories in the simulation. In this work, the MD simulations were performed by using an appropriately modified version of the Large Atomic Molecular Massively Parallel Simulator (LAMMPS). It is a classical molecular dynamics open-source code written in C++ and developed by Sandia National Labs. [29]

Table 1: Implementation of Hybrid Interface on CFD and MD Codes. Both codes are equipped with the file-based information exchange routine, to update the hybrid boundary condition. CFD code experiences the global change of its data structure to store the information of the entire fluid system. MD code adopts hybrid equations to impose the macroscopic information on microscopic domain and to ensure numerical stability.

	CFD	MD
Global Change	Overset Data Structure (*optional)*	-
External Force	-	External Force Equation (Eqn. 4)
CFDtoMD	File Interface: Sender	File Interface: Receiver Constrained MD Equation (Eqn. 10)
MDtoCFD	File Interface: Receiver	File Interface: Sender

2.3. Hybrid Interfaces and Schemes

The hybrid simulation requires the implementation of hybrid interfaces and schemes on individual code. In the current study, the file interface is designed to schedule the information exchange between continuum and discrete particle descriptions. A constrained Lagrangian dynamics model is implemented for hybrid simulation. Unit conversion routine is also implemented in the application code. These changes are summarized in table 1.

The CFD code employs the data structure of overset mesh technique [25] to ease the handling of coupling parameters. In other words, the entire fluid domain is generated as the CFD mesh system and pure MD region is turned off as the 'Hole' cell in the terminology of overset technique. Likewise, MDtoCFD and CFDtoMD boundary cells are declared as 'Fringe' and 'Donor' cells, respectively. The labor of mesh regeneration according to the change of coupling parameters (position and depth of hybrid layers) disappears with the overset data structure.

Both codes are equipped with the information exchange routine which consists of one file sender and one file receiver. These file interfaces are scheduled to turn on every sampling interval. The instantaneous properties in the Donor cells of continuum domain are transferred to MD site and referenced when applying constrained Lagrangian dynamics equation. Aver-

aged molecular properties are sent to CFD domain and they are used as the boundary conditions of Fringe cells. All exchanged properties are written in MD unit: thus, CFD code is equipped with velocity unit conversion function and equation of state which changes the pressure solution from CFD site to equivalent density property in MD domain.

Along with the file interface, additional equations of motion are employed on MD code to accurately describe the influence of macroscopic flow variation on particle domain. First, the external force should be imposed to prevent leaving particles from the control domain and the force is applied to the normal direction of uppermost MD layer. A cost-effective classical external force model by Nie *et al.* [2] is employed as,

$$F_{ext,i} = -p_a \sigma \frac{y_i - Y_{n-1}}{1 - (y_i - Y_{n-1})/(Y_n - Y_{n-1})} \tag{4}$$

where p_a denote the average pressure in the MD region, $Y_n - Y_{n-1}$ is the thickness of the uppermost layer which is applied the force and F_{ext} is the external force acting on i^{th} particle located on position y_i.

Next, on CFDtoMD layer, the macroscopic flow properties at specific time shall be introduced to lead the motion of multiple particles in that layer. To satisfy mass conservation, a certain number of particles are inserted into or removed from this layer according to the mass flux by CFD solution,

$$n = -A\rho u_y \Delta t / m \tag{5}$$

where A is the horizontal area, u_y is the vertical velocity component by CFD solution and Δt is the sampling interval.

A very complicated numerical intervention is required to maintain momentum conservation. The average velocities of particles in J_{th} cell is equal to the velocity u_J in continuum cell.

$$u_J(t) = \frac{1}{N_J} \sum_i v_i \tag{6}$$

where v_i is velocity of i^{th} particle and N_J is the number of particles in the cell. With taking Lagrangian derivative of Eq. 6,

$$\frac{Du_J(t)}{Dt} = \sum_i \frac{\ddot{x}_i}{N_J} \tag{7}$$

The Classical MD equation of motion can be generalized to obtain constraint by adopting the fluctuation in acceleration of each particles, ζ_i

$$\frac{F_i}{m_i} = \ddot{x}_i(t) = \frac{Du_J(t)}{Dt} + \zeta_i = \frac{\sum_i F_i(t)}{\sum_i m_i} + \zeta_i \tag{8}$$

where F_i is the force on i^{th} particle based on the interactions between particles, m_i is mass of each atom and Eqn. 9 satisfies,

$$\sum_i \zeta_i m_i = 0 \tag{9}$$

Finally, the constrained particle dynamics with conventional equation of motion can be written as:

$$\ddot{x}_i(t) = \frac{F_i}{m_i} - \frac{\sum_i F_i(t)}{\sum_i m_i} - \frac{1}{\Delta t_{MD}}\{\frac{\sum_i m_i \dot{x}_i}{\sum_i m_i} - u_J(t + \Delta t_{MD})\} \tag{10}$$

The continuum velocity and the mean microscopic velocity from MD over control domain provide the synchronization of the mass and momentum consistent with Eqn. 10.

2.4. Statistical Error and Coupling Parameters

How to reduce the statistical error of averaged MD profile, which is the response of innate spatial/temporal locality in molecular dynamic systems, determines the accuracy of CFD solution in hybrid simulation. According to the mathematical expression in statistical error [10, 17], the ratio of sampling noise compared to the macroscopic velocity is inversely proportional to the square root of spatial layer size and temporal sampling duration. For example, reducing the macroscopic velocity by half requires either 4 times larger system domain or 4 times longer sampling to maintain the same order of accuracy.

Sampling duration with interval, the size of sampling layer and its position are coupling parameters which define the scale and pattern of this noise. The layer size and sampling duration collectively work for reducing the noise, by increasing the spatial and temporal sampling scales. Sampling interval is a factor which restricts the sampling duration. On unsteady simulations, a

short sampling interval is preferred to frequently update temporal variation of flow field in hybrid boundary zones. This interval acts as the upper bound of sampling duration. The location of the sampling layer is a secondary factor which can locally increase the strength of fluctuation. Conventionally, sampling layer is placed far from the solid obstacle, e.g., at least 10 σ above the bottom wall in solving the flow of the liquid argon [6].

We introduce two numerical ideas to acquire the accurate hybrid solution. One is to quantitatively measure the scale of statistical noise in particular domain and the other is to numerically get the acceptable solution. The former shows the initial guideline to determine the coupling parameter and the latter refines the accuracy of the former solution.

2.4.1. Determining Coupling Conditions

The statistical noise is a function of the characteristics of fluid and surrounding solid elements, and geometric configurations, as well as the flow condition. Unfortunately, previous analyses on the strength of statistical error [10, 17] fails to consider the stronger interaction near the fluid-solid interface and the shape of the domain. We sense that the clear coupling parameters can be determined after the look-up of that specific system

Our intuitive idea of numerically detecting the strength of statistical noise is to solve the stationary flow of the same fluid domain by pure MD method. The procedure is as follows.

1. Empirical design of the sampling interval and the sampling layer's position[1]
2. Structure construction[2]
3. Simulation and collecting the temporal history of sampled velocity[3]
4. Data processing[4]
5. Determining the sampling layer size and the sampling duration[5,6]

We argue that our idea is very easy to follow and computationally not expensive since the solution of the stationary flow is immediately collected. This stationary flow simulation provides the amount of sampling noise in various sampling conditions. Meanwhile, this experiment does not provide the statistical error because of the impossibility to predict the macroscopic velocity expect some well-known flow systems. This necessitates us to investigate additional approach which is globally applicable.

2.4.2. Sampling Multiple Independent Experiments

So far, all hybrid CFD-MD applications have been restricted to extremely fast flow field of O(100) m/s velocity. The difficulty of solving moderate-speed flow field by a hybrid approach is explained as follows. The hydrodynamic time scale is expressed as a function of characteristic size and kinematic viscosity. This implies that the sampling interval is fixed regardless of the change in velocity. This, in turn, results in the impossibility to handle the sampling duration. Increasing the system size proportional to the square of the velocity change remains the only possible way to maintain the same statistical accuracy. Unfortunately, submitting excessively large-scaled simulation on public supercomputers unfavorably takes far long time to get allocated. In worse case, the simulation may exceed the capacity of the system. Thus, a

[1]Sampling interval is designed less than $1/100^{th}$ of hydrodynamic characteristic time; The location of sampling layer is placed O(10) nanometers above the solid obstacle.

[2]The height of the domain can be reduced by placing a specular wall on the top, in case the system is sufficiently large; The length of the domain along the periodic direction can be arbitrarily chosen. The optimal length is further determined by the relation between the strength of noise and number of particles, i.e., $V_{noise} \propto 1/\sqrt{N}$.

[3]Data collection starts as soon as the relaxation process is finished. Temporal history of averaged velocity from the smallest layer size with shortest sampling interval is stored.

[4]Produced dataset around the location of sampling layer is spatially and temporally averaged to produce the spatial and temporal variation of the sampled velocity.

[5]The noise is compared with the expected macroscopic velocity at that position, considering the linear velocity gradient from the wall to the far field. A paired condition which produces sufficiently small portion of noise and whose temporal duration is less than designed sampling interval is chosen to be the layer size and sampling duration of this hybrid simulation.

[6]If no condition is satisfactory, the acceptable condition can be obtained by either increasing the length of computational domain based on $V_{noise} \propto 1/\sqrt{N}$ or changing the position of sampling layer and repeating data processing. The one condition which generates the smallest MD domain in the hybrid simulation is chosen.

different approach is necessary for efficiently simulating the low-speed flow field.

We propose sampling multiple independent hybrid simulations from a smaller domain instead of trying to run a single hybrid simulation in the large domain. The initial velocity component at individual problem set is differently determined from a Maxwell-Boltzmann distribution and solutions from independent simulations are averaged to produce the final solution. The labour of manually administrating multiple job executions are resolved by using a BigJob framework, which is to be discussed in the Section 3.

Along with the advantage in computing capability, sampling multiple experiments provides another advantage of less-sensitivity to coupling conditions. Even if the coupling parameters are ill-chosen, highly noisy individual solution can be refined by the enough number of independent samples. This advantage also increases the value of capturing the magnitude of statistical noise in Section 2.4.1, because the requirement of predicting the macroscopic velocity in the sampled layer becomes less important.

2.5. Temporal Coupling Schemes

Two conventionally used coupling approaches of synchronized and sequential coupling strategies are depicted in Fig. 2. In synchronized coupling, CFD and MD codes exchange the information in the overlapping region at each sampling interval (denoted by Δt) and independently evolve to the next exchange time step. In contrast, one domain advances to the next exchange time step and leads its counterpart to approach this point in sequential coupling. Comparing these two mechanisms, synchronized coupling has a far better parallel efficiency because both codes independently evolve to the next sampling interval, while sequential approach is expected to produce more time-accurate solution because the boundary condition on following domain (CFD domain in the figure) is implicitly imposed. Unfortunately, both strategies contain the time-lagging phenomenon in CFD boundary region, because averaged molecular dynamic properties over backward sampling duration (from $n\Delta t - \Delta t_s$ to $n\Delta t$) represents the CFD boundary condition at that instance ($n\Delta t$). Extrapolation from previous MD solutions is necessary to eliminate the time-lagging by half of sampling duration ($\Delta t_S/2$) in the CFD boundary zone.

As is presented in Fig. 3-(0), Wang and He [5] proposed shifting the time axis of one domain by half of the sampling interval to eliminate this lagging effect. After both codes evolve by a sampling interval, the instantaneous CFD

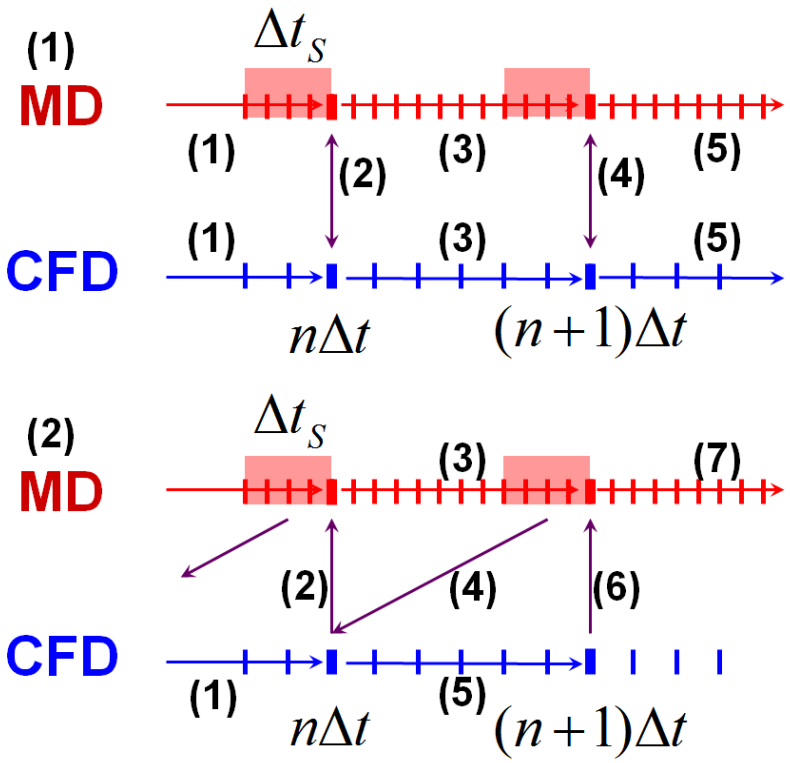

Figure 2: Conventional Time Evolution Mechanisms of a Hybrid CFD-MD Approach; CFD and MD codes are scheduled to conduct data exchange in the overlapping region at every Δt sampling interval. CFD solution at $n\Delta t$ is directly applied as the boundary condition for MD simulation and backward time-averaged molecular dynamic properties over Δt_S sampling durations are imposed as CFD boundary conditions. (1) Synchronized Coupling: Both codes communicate at the same time level and independently iterate to next exchange point. (2) Sequential Coupling: From the same time level, one solver advances to the next communication point and impose implicit boundary condition to its counterpart.

solution at $n\Delta t$ is communicated with averaged MD solution from $(n-1/2)\Delta t$ to $(n+1/2)\Delta t$. Two previous solutions from the counterpart are extrapolated to impose hybrid boundary conditions. The benefit of imposing extrapolated boundary condition is that the sampling duration can be designed as long as the sampling interval ($\Delta t_s = \Delta t$). However, the accuracy of extrapolated solution is worth to debate. In this scheduling, two *previous* CFD solutions at $(n-1)\Delta t$ and $n\Delta t$ are extrapolated to produce MD boundary conditions from $(n+1/2)\Delta t$ to $(n+3/2)\Delta t$. Except the velocity gradient is linear in time space, extrapolated properties fail to predict correct values throughout the simulation interval (from$(n+1/2)\Delta t$ to $(n+3/2)\Delta t$). The only way to reduce this extrapolation error is to reduce the sampling interval, which is contradictory to the condition for reducing the statistical error.

A new scheme named 'prediction-correction approach' is also depicted in Fig. 3. The main difference from the default model is that CFD code iterates additional time steps after the code evolved to the next data exchange time. For example, in Fig. 3-(1), CFD code additionally evolves by the half of sampling interval after the code approached to $n\Delta t$. CFD code sends these predicted properties at $(n+1/2)\Delta t$ to the MD site and receives averaged molecular properties around $n\Delta t$. CFD code loads its previous flow profile at $n\Delta t$ and runs the actual simulation to next communication point at $(n+1)\Delta t$. Clear benefit of current approach is that both solvers extrapolate their boundary conditions from *current* solutions (either exact solution or predicted values) instead of using *previous* history. This eliminates the sensitivity of extrapolated solution according to the size of sampling interval in previous model, which enables increasing the sampling interval.

This approach is further refined to increase the accuracy of the hybrid boundary condition by increasing prediction time scale. In Fig. 3-(2), the prediction time scale is increased by one more sampling interval. While MD solver evolves for one sampling interval, CFD code iterates to the next communication point of MD time space. This enables MD boundary condition being interpolated by predicted CFD profiles. Figure 3-(3) demonstrates the imposition of interpolated boundary conditions on both domains. In this formulation, CFD time space is shifted backward by one sampling interval and prediction step is scheduled to be $(5/2)\Delta t$.

Current numerical approach provides more accurate time-variant solution by decreasing or eliminating the unfavorable overshoot/undershoot phenomena in extrapolations. Meanwhile, additional computational cost is inevitable for CFD simulation. We propose the current approach to be used in following

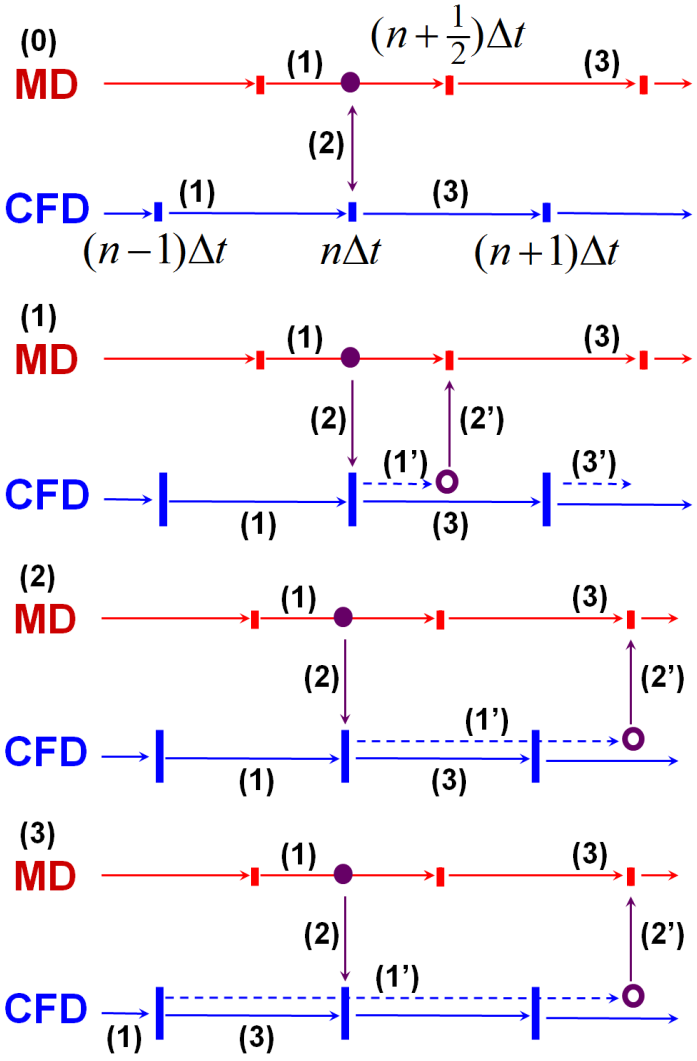

Figure 3: A Prediction-Correction Approach with Extrapolated/Interpolated Hybrid Boundary Conditions; Applying extrapolation/interpolation enables increasing sampling duration as long as sampling interval. (0) Default Formulation; The hybrid BC in MD code is extrapolated from previous solutions. (1) Extrapolated Boundary; CFD code runs the prediction step by $0.5\Delta t$. MD code imposes the hybrid BC by the extrapolation from the current value. (2) Interpolated MD Boundary; CFD code runs the prediction step by $1.5\Delta t$. MD code imposes interpolated hybrid BC. (3) Interpolated Hybrid Boundary Conditions; Time axis of CFD domain shifts back by 1 sampling interval and the prediction step is set $2.5\Delta t$. CFD and MD domains impose interpolated hybrid BC.

conditions: (i) computational cost on CFD is quite smaller than that of MD, and (ii) the driving force which causes the flow variation is provided from the CFD domain. Without condition (i), additional computational overhead for prediction process will harm the simulation performance. If (ii) is not satisfied, the pattern of flow evolution cannot be predicted and the accuracy of the predicted solution is not guaranteed.

3. Coupled Concurrent Multi-Scale (Continuum-Molecular) Simulation Framework

Two important issues on the performance of hybrid simulations are co-scheduling and load-balancing. Both can be resolved by adopting a Pilot-job concept. We explain the design of a multi-physics simulation framework which operates in the form of a single Pilot-job and contains a load-balancing function between distinct tasks.

3.1. SAGA and SAGA-based Frameworks - An Efficient Runtime Environment for Coupled Multi-component Computations

The Simple API for Grid Applications (SAGA) [26] is an API standardization effort within the Open Grid Forum (OGF) [27], an international standards development body concerned primarily with standards for distributed computing. SAGA provides a simple, POSIX-style API to the most common Grid functions at a sufficiently high-level of abstraction so as to be independent of the diverse and dynamic Grid environments. The SAGA specification defines interfaces for the most common Grid-programming functions grouped as a set of functional packages (Fig. 4). Some key packages are:

- File package - provides methods for accessing local and remote filesystems, browsing directories, moving, copying, and deleting files, setting access permissions, as well as zero-copy reading and writing
- Job package - provides methods for describing, submitting, monitoring, and controlling local and remote jobs. Many parts of this package were derived from the largely adopted DRMAA
- Stream package - provides methods for authenticated local and remote socket connections with hooks to support authorization and encryption schemes.

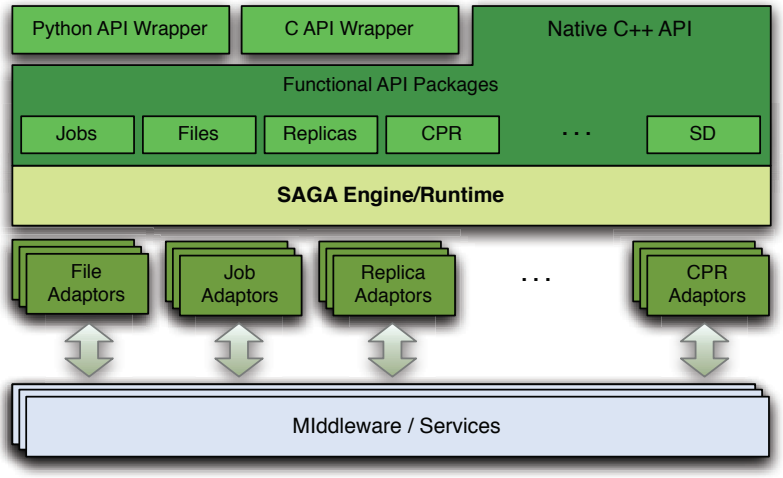

Figure 4: Layered schematic of the different components of the SAGA landscape. At the topmost level is the simple integrated API which provides the basic functionality for distributed computing. Our BigJob abstraction is built upon this SAGA layer using Python API wrapper

- Other Packages, such as the RPC (remote procedure call) and Replica package

The BigJob [28] is a SAGA-based Pilot-Job, where a number of sub-tasks (called as "sub-jobs") can run in a pre-defined schedule with the specified number of cores (or processors; we use the term "core" to represent a single processing element) whether or not they are coupled. We basically devise this solution to overcome the concurrent scheduling requirement of coupled CFD and MD sub-jobs and to dynamically allocate resources for load-balancing of these codes. The advantage of a BigJob over other Pilot-Job implementations is that this is infrastructure-neutral, thanks to various adaptors in SAGA.

Fig. 5 shows the structure of BigJob and its operation flow. When a BigJob is submitted to the remote resource, the application manager monitors the status of this Pilot-Job through the advert service. When resources are allocated to the BigJob, the application manager allots the obtained resources to its sub-jobs and a coupled simulation starts under the control of a multi-physics agent in the remote resource. Advert service keeps on getting the status of a Pilot-Job from the queuing system and the status of

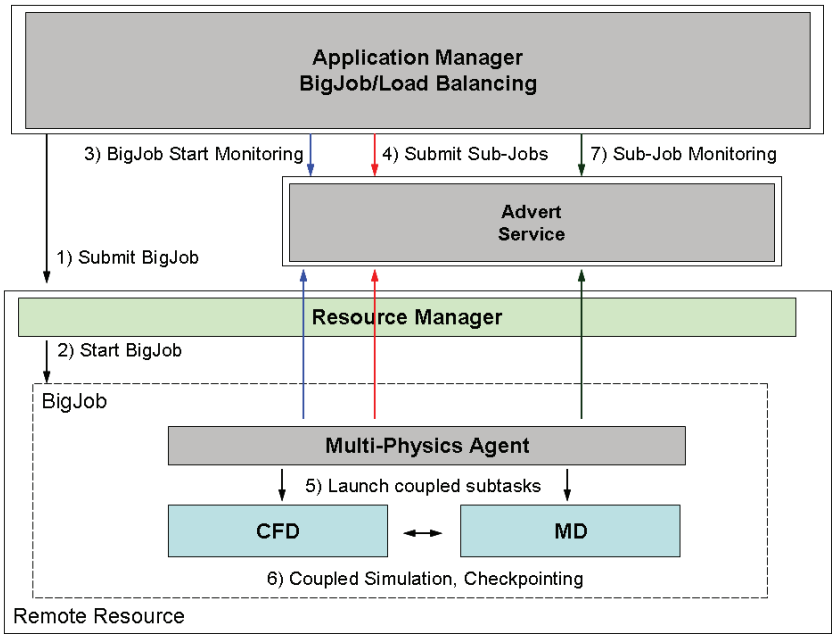

Figure 5: Architecture of the Controller/Manager and Control Flow: Application manager is responsible for job management including BigJob and sub-job submission, their status monitoring functions. We implement a load-balancing module, and migration service based on job information. Application agent system resides on each HPC resource and conducts job information gathering and also communicates with the application manager via the advert service

sub-jobs from multi-physics agent. It also delivers this information to the application manager by a push-pull mechanism. The application manager watches the status of sub-jobs and decides the next event when the coupled simulation is finished. If an individual simulation is of interest, the manager closes a BigJob allocation when the simulation is finished: In cases of multiple replica simulations or load-balanced coupled simulation, the manager relaunches sub-jobs on the same BigJob allocation until all replicas or simulation loops are completed.

3.2. Load-Balancing of Coupled Multi-Physics Simulation

Load-balancing of a coupled simulation implies the flexibility to re-distribute resources to the individual job according to each performance. We will discuss the implementation and algorithm of a simple load balancer (LB) [29]; it is important to mention that the LB functions in the context of the SAGA-

BigJob framework.

The idea is to assign more resources to heavier sub-jobs under the fixed resource allocation, until all sub-jobs elapse the same execution time. As it is impossible to predict the performance of each code in advance, we let the LB monitor the wall-clock time between information exchange points of coupled sub-jobs and iteratively change the resource distribution until the load-balancing is achieved. As the individual solver is considered as black-box, each application code is assumed to have the ideal parallel efficiency: In case application codes are highly scalable, the LB can find the best condition after a few dynamic re-distributions. Also, all cores in one node are assigned to one single task to prevent the interference (and performance degradation) observed when multiple MPI tasks share the node.

Let the computation time (between exchanges) of the two sub-jobs be t_{CFD} and t_{MD}, and the number of cores assigned to each domain be PE_{CFD} and PE_{MD}, respectively. Subscripts C and N denotes current and next states. Assuming ideal parallel efficiency, total load of each application remains the same after resource re-allocation,

$$\begin{aligned} W_{CFD} &= PE_{CFD,C} \times t_{CFD,C} = PE_{CFD,N} \times t_{CFD,N} \\ W_{MD} &= PE_{MD,C} \times t_{MD,C} = PE_{MD,N} \times t_{MD,N} \end{aligned} \tag{11}$$

In spite of the re-allocation, the total number of cores utilized remains the same:

$$PE_{TOT} = PE_{CFD,C} + PE_{MD,C} = PE_{CFD,N} + PE_{MD,N} \tag{12}$$

Our objective is to reduce the computation time of a sub-job to the point until the two application components show the same computation between the exchange points, i.e., $t_{CFD,N} = t_{MD,N}$. From Eqn. 11 and Eqn. 12 an optimal number of cores distributed for the CFD sub-job would be:

$$PE_{CFD,F} = \frac{W_{CFD}}{(W_{CFD} + W_{MD})} \times PE_{TOT} \tag{13}$$

The MD simulation (sub-job) will follow a similar expression.

The above non-integer value proceed in discrete values expressed as the multiples of the number of CPU cores in a node. We choose the nearest discrete number to our load-balancing as the optimal number of core on each application.

3.3. Implementation of an Execution Framework and Application-level Corrections

A hybrid CFD-MD framework is evaluated by implementing an application manager in Fig. 5, which is written in PYTHON script language. By default, an application manager calls a number of SAGA functions in sequence, to get allocated a vacant job, to run individual MPI simulation, to monitor its status, and to finalize the BigJob allocation.

In case the load-balancing capability is turned on, the situation becomes complicated. A single MPI job is not able to change its number of cores during the simulation. This implies that coupled codes should stop-and-restart to get assigned with changed number of cores. Thus, sub-jobs are scheduled to have multiple restarts from the previous checkpointing solution, which we denote 'simulation loop'. A LB is serviced as a separate function in an application manager and is scheduled to run in between each restart of sub-jobs.

The efficient functioning of the LB is predicated on application codes being able to restart from their checkpointing data effectively. Application codes should also be equipped with generalized domain partitioning routine to run a simulation with any number of cores, without harming their parallel efficiency a lot. Another change implemented on application codes is the time checking routine. The runtime of each application is meaningless in running a LB since this runtime contains idle waiting on inter-domain information exchange as well as the individual simulation time. This actual runtime can be counted by putting two wall-time functions before and after the information exchange routine.

The generation of an application manager and the changes in application codes raise the possible simulation scenarios as given in Fig. 6. The first (leftmost) shows the time evolution of a coupled simulation under a conventional job submission (which we define to be scenario S0), and others using a BigJob (denoted as S1). For S0, individual tasks with resource requirements of PE_{CFD} and PE_{MD} respectively, are independently submitted to the conventional queuing system and job scheduler recognizes these coupled tasks as two distinct jobs. Thus, they start at different times on average. In this case, both tasks wait on the queue when no job is allocated (waiting stage), the first allocated job idles to perform data exchange with its counterpart (idling stage), and the actual simulation starts when both jobs are allocated (running stage). On the other hand, for scenario S1, a BigJob of size $PE_{CFD} + PE_{MD}$ is submitted to the queue, and coupled simulation

directly starts when the resource is assigned to this BigJob. Because of co-scheduling of sub-jobs, a BigJob is free from long inactive mode which is frequent in conventional job submission, while total runtime is the same if the resource distribution to sub-jobs is identical. However, eliminating inactive mode in itself does not guarantee a reduction in the total runtime, because a larger single allocation may result in a greater queue waiting time than two simulations requesting smaller number of cores each (but the total being the same). The same situation can arise for the load-balanced case with one BigJob ($S1_{LB}$). From the comparison between S1 and S0, we can estimate the performance gain by concurrent start of distinct coupled codes; $S1_{LB}$ solution compared to other scenarios will demonstrate the benefit of a load-balancing function on coupled simulation.

4. Multi-physics Flow Simulations in Various Flow Conditions

A hybrid CFD-MD framework is employed to solve the multi-physics flow in nano-scale. Experimented problems are a sudden-start Couette flow and the oscillating boundary problem. We start from determining coupling parameters to the validation and verification of the hybrid simulation framework, then to the exploration of the moderate-speed flow simulation and time-accurate hybrid simulation.

4.1. Problem Description and Coupling Conditions

All applications we examine are internal flow fields filled with the liquid argon. Characteristic length of liquid argon is $\sigma = 3.405\times10^{-10}$ and time scale is $\tau = 2.2\times10^{-12}$. Density is $0.81m\sigma^{-3}$, which means 0.81 atoms are included in the characteristic volume. The fluid domain is a channel system which consists of two parallel plates placed in vertical direction. Liquid argon particles are filled in the domain and both walls have artificial properties which is the same as those of liquid argon. The slip ratio between fluid and solid particles are set 0.6, to satisfy the linear velocity gradient along the vertical direction. [2] Channel is 52 σ in height, which is $O(10^{-8})$ meters. Applications covered in this work are periodic systems in the perpendicular direction and the flow variation is derived by the horizontal motion of an upper plate.

As has been proposed in Sec. 2.4.1, we solve a stationary flow in particle domain to determine coupling conditions. Table 2 shows the averaged velocity depending on the layer size and sampling duration in 10^{-8} meter domain.

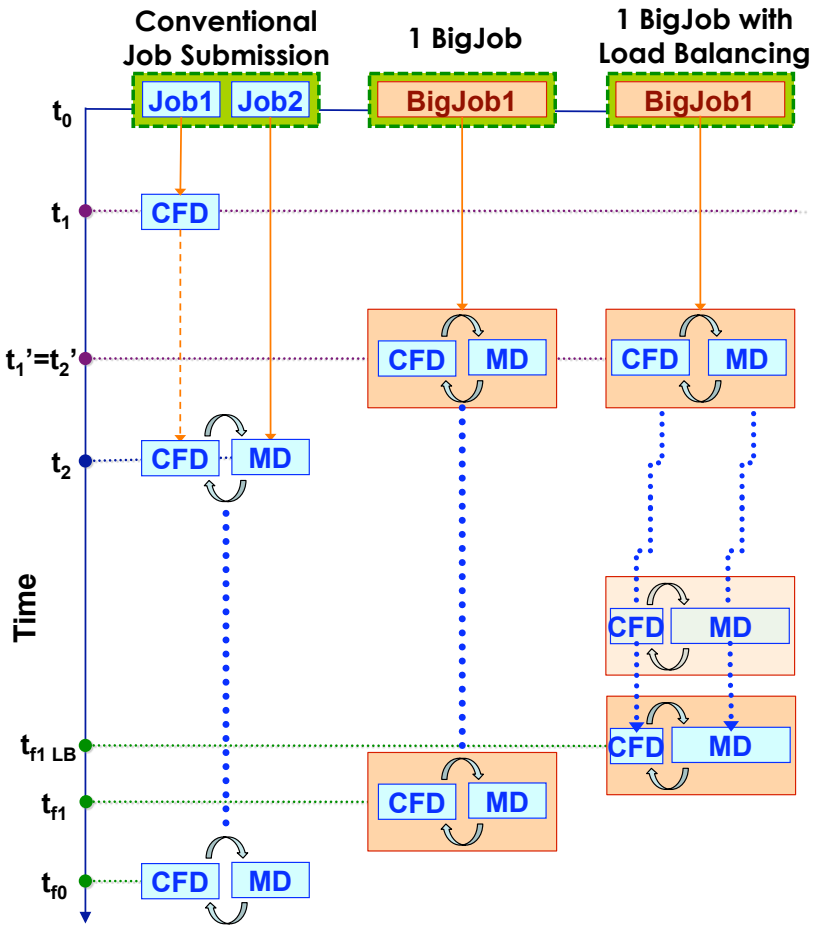

Figure 6: Comparison of dependencies encountered for coupled simulations submitted as conventional jobs, to the scenario when using Pilot-Jobs. Here we use only 1 BigJob (S1). The conventional mode of submission experiences three phases based upon their queue state: (i) All jobs are waiting: $(t_1 - t_0)$; (ii) Inactive mode (where one job is waiting for another: $t_2 - t_1$), and (iii) Active mode (running a coupled simulation: $t_f - t_2$). The Inactive stage, disappears when a coupled simulation runs within a BigJob, as an allocated BigJob distributes its resource to both sub-jobs.

Experiments were conducted with different lengths of the domain, changing from 35 σ to 70 and 140 σ. Noises around 0.2 height above the wall are presented.

From the individual test, we find that mathematical expressions on the strength of noise according to the height of sampled layer and sampling duration [10, 17] do not coincide with our experiment. From the first table, increasing the height of averaged layer from 0.1 to 6.4 σ reduces the statistical error by 4 times when sampling duration is 1 τ and this ratio even gets worse as sampling duration increases. The same situation also happens on sampling duration. This is contradictory to previous mathematical expressions which has been introduced in Sec. 2.4. From the data analysis, we figure out that the magnitude of sampling noise depending on the layer size and sampling duration is far more complicated: $V_N = a \times SD^b \times LH^c \times SD^{d \times ln(LH)}$, where V_N represents the velocity magnitude of the noise, SD denotes sampling duration and LH is the height of the layer. This equation is rewritten in simpler logarithmic formulation as,

$$ln(V_N) = ln(a) + b\ ln(SD) + c\ ln(LH) + d\ ln(SD)\ ln(LH)$$

and these coefficients in our specific case are as,

$$\begin{aligned} L = 35\sigma: &\quad a = 33.67,\ b = -0.18,\ c = -0.30,\ d = 0.052 \\ L = 70\sigma: &\quad a = 25.85,\ b = -0.19,\ c = -0.27,\ d = 0.062 \\ L = 140\sigma: &\quad a = 17.78,\ b = -0.18,\ c = -0.25,\ d = 0.060 \end{aligned}$$

which directly expresses that 4 times longer sampling duration or 4 times larger layer height is far insufficient to half the noise.

Another result we observe from the above mathematical expression is that increasing the system size into the periodic direction is more effective in reducing the noise. Setting SD and LH to 1 τ and 1 σ, we find that the magnitude of the noise reduces from 33.67 to 17.78 if system size is quadrupled. This result supports previous mathematical expressions on statistical error.

Following conclusions are deduced from the sampling noise analysis in the stationary flow. First, previous analyses on statistical error cannot be applied on wall-bounded nanoscale systems. As our empirical equation presents, the layer height and sampling duration are coupled together and noise reduction by handling these factors are less effective than have been reported. This emphasizes that the actual measurement of the sampling noise is inevitable to

Table 2: Statistical Error in Stationary Flow Simulation; Pure MD simulations of 35 $\times$ 52, 70 $\times$ 52 and 140 $\times$ 52 σ^2 are conducted. Liquid is bound in Y-direction by upper and lower walls and able to move in X-direction where periodic boundary condition is imposed. Initial data up to 100 τ are disregarded to provide enough time for minimization. Velocity of particles around the central layer are accumulated over 512 τ by using *fix-ave-spatial* function in LAMMPS package and post-processed to get the average velocity at different layer size and sampling duration conditions. Statistical noise becomes about half at 4 times bigger domain. The unit is 1/1000 of non-dimensional MD velocity (1σ / τ).

	1 τ	2 τ	4 τ	8 τ	16 τ	32 τ	64 τ
0.1 σ	62.332	48.396	40.245	35.006	26.761	21.605	17.617
0.2 σ	53.821	43.877	36.693	32.067	24.108	20.874	18.912
0.4 σ	46.200	38.967	33.122	29.881	24.044	19.666	18.827
0.8 σ	40.087	35.490	31.412	28.671	23.949	20.382	19.255
1.6 σ	32.455	30.470	27.382	24.405	20.140	17.494	16.594
3.2 σ	23.019	21.877	21.072	18.534	16.532	14.395	13.643
6.4 σ	16.113	15.754	15.289	14.649	13.459	12.909	12.858

	1 τ	2 τ	4 τ	8 τ	16 τ	32 τ	64 τ
0.1 σ	44.207	34.909	28.885	23.981	17.466	12.986	12.630
0.2 σ	36.675	31.260	25.690	22.203	18.914	12.341	11.695
0.4 σ	32.370	28.093	24.062	19.818	17.875	12.819	11.980
0.8 σ	29.544	26.477	23.613	19.966	18.261	13.404	12.521
1.6 σ	24.729	22.964	21.099	19.111	17.878	14.058	12.684
3.2 σ	18.719	18.102	17.111	16.487	15.723	13.074	12.115
6.4 σ	12.791	12.596	12.388	12.121	11.723	10.311	9.536

	1 τ	2 τ	4 τ	8 τ	16 τ	32 τ	64 τ
0.1 σ	30.578	24.249	19.228	15.659	13.238	10.163	9.308
0.2 σ	26.803	21.931	18.138	14.721	11.844	10.045	8.494
0.4 σ	23.158	19.426	16.965	13.620	10.759	9.742	8.355
0.8 σ	20.055	17.501	15.703	13.378	10.527	9.796	8.069
1.6 σ	15.966	14.691	13.486	11.888	9.944	9.398	8.034
3.2 σ	12.584	12.144	11.623	10.484	9.755	9.295	8.376
6.4 σ	10.243	10.091	9.860	9.662	9.189	9.059	8.117

determine coupling parameters in the specific system. Second, increasing the size of sampling layer in the periodic direction is more effective on reducing the sampling noise. This leads us to an unfavorable conclusion that additional computational cost should be sacrificed to get the acceptable sampled solution.

Finally, CFD and MD computational domains are generated based on the above experiment, as depicted in Fig. 7. Pure MD region is specified to be 10σ, which was reported to be sufficient to prevent strong fluctuation between fluid particles and wall materials from directly transported to CFD domains. [6] This implies that the steady-state velocity in the hybrid domain will be around 0.2 σ/τ. We design the strength of the statistical error not to exceed 5 percent ($\approx$ 0.01 σ/τ) of steady-state velocity. This lead us to set the width of MD domain in the principal flow direction as 140 σ, the cell size of CFD mesh to be 2σ in Y-direction, and sampling duration to be 10 τ. Two layer boundary zones from particle to continuum domain is placed ahead of pure MD region, from 10 to 14σ. Two layers of continuum to particle boundary is positioned from 18 to 22σ and external force region is place at the top of hybrid region, from 24 to 26σ.

4.2. A Sudden-start Couette Flow

A sudden-start Couette flow is simulated to verify the accuracy of the current framework with multiple sampling approach for the moderate-speed flow simulation. This application has been in wide use for the validation of a hybrid CFD-MD solver. [2, 6] The flow is initially set stationary and the upper wall starts moving by a constant velocity (1 σ/τ). This physical boundary condition of the continuum domain governs the evolution of the whole flow field. Figure 8 presents a sudden-start Couette flow profile by CFD, MD and hybrid simulations. Pure CFD produces identically the same result as analytic solution and MD simulations also describes the same flow physics though the slight fluctuation of the solution is observed. This verifies the accuracy of the individual solver. The hybrid solution also shows the slight deviation from the analytic solution, which is the fluctuation of the sampled MD solution. Nevertheless, the hybrid simulation succeeds in demonstrating the same flow physics as the analytic solution. This variation can even be diminished if the solution is visualized over a longer temporal range, which is observed in many articles. This proves that the current hybrid framework accurately analyzes the steady flow profile in nano-scaled systems.

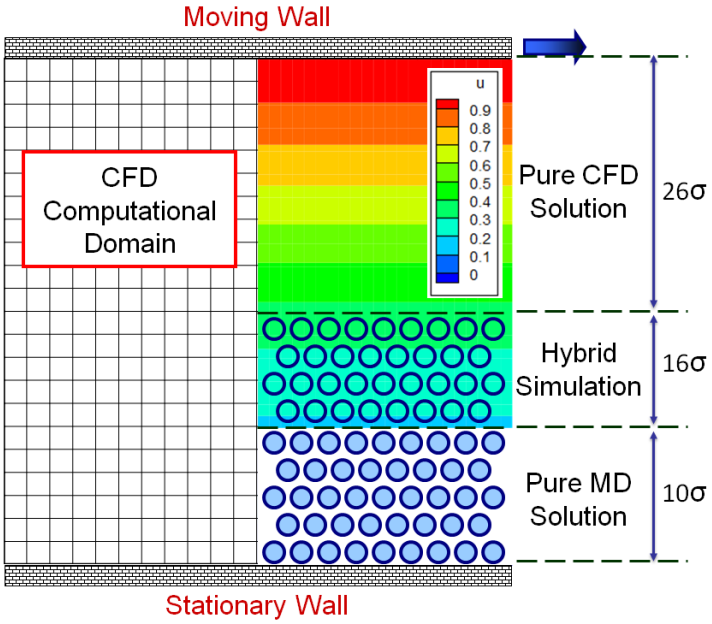

Figure 7: Computational Domain of Couette Flow Simulation; The height of the fluid domain is 52σ ($\approx 177\mathring{A}$). CFD mesh size is 71×27 and CFD cells at the pure MD region are treated as holes. MD domain size is about 140σ in the X-direction and around 26σ in the Y-direction, including the bottom wall. Periodic boundary condition is applied on the principal flow direction.

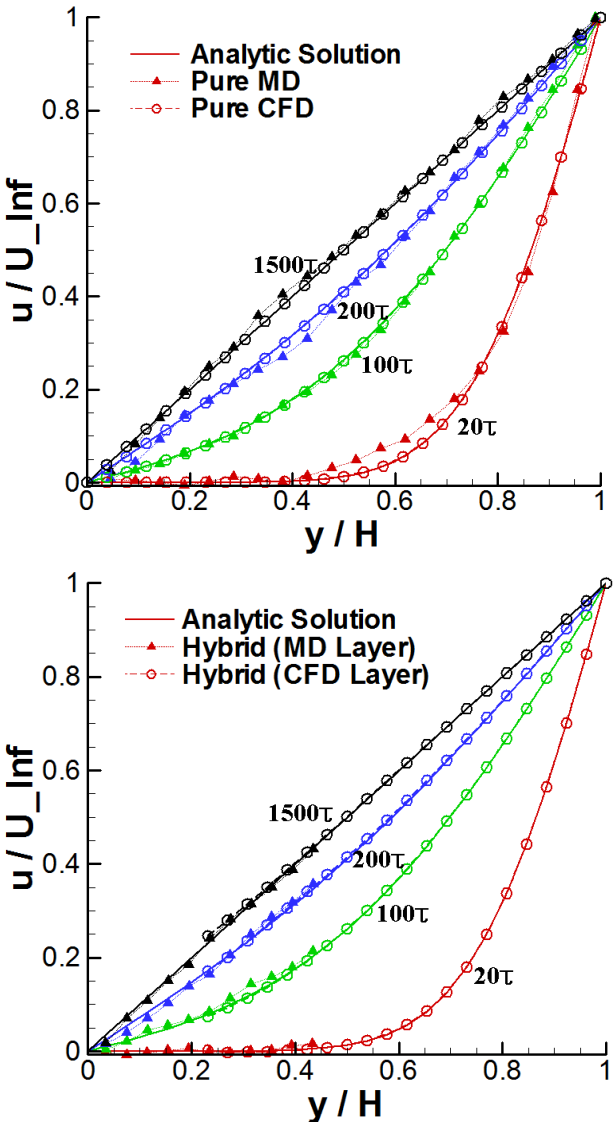

Figure 8: Unsteady Couette Flow Profile; The evolution of velocity field along the vertical direction is presented. CFD solution is the instantaneous profile at specified time and MD solution is spatially averaged over 2 σ in height and temporally averaged for 1 sampling durations (=10τ). (Left) Pure CFD solution is exactly the same as analytic solution. MD solution shows the same flow pattern as analytic solution, though some fluctuation is observed. This verifies that CFD and MD represents the same flow physics. (Right) The steady result by hybrid approach produces the same numerical result as analytic solution, though the slight time-lagging in the hybrid boundary is observed during the evolution.

The flow condition in above experiment is rather unrealistic, which motivates us to apply the hybrid scheme to the analysis of moderate velocity flow. As has been expressed in Sec. 2.4.2, hybrid simulation of the low-speed flow field is mathematically possible but technically bound by the computing capacity, since the computational domain becomes u^2 times bigger in solving $1/u$ velocity field. We instead run u^2 independent simulations with the initial system size and different random number seeds in LAMMPS package.

The Couette flow profile with different numbers of samples are presented in Fig. 9. All configurations and parameters are identical to the above validation problem, except the upper plate velocity of 0.25 σ/τ. Changing the velocity to 1/4 implies that averaging 16 samples are required to get the acceptable numerical solution. The result supports the above supposition. The solution becomes very accurate when 16 individual runs are sampled. The reduction of statistical noise by multiple samplings is clearly verified by the graph in Fig. 10. The noise is roughly seen to reduce by half with 4 times more samples and the solution of sampling 16 runs shows about 5 % of the noise compared to the analytic solution profile.

The solution by multiple sampling is compared with the solution in increased system domain. Figure 11 shows the Couette flow profile with 16 times bigger system size in horizontal direction and the comparison of velocity variation in the middle of the overlapping region. From the result, both ways (multiple sampling and increasing system size) produce acceptable numerical solutions compared to the analytic solution. Interestingly, the scale of the noise compared to the analytic solution is very similar in both ways, which verifies that multiple sampling approach can replace the increase of system size to reduce the statistical error.

Collectively, results by multiple samples show the same order of accuracy compared to the increase of the system size. Especially in cases the physical system is large, multiple sampling is more effective than directly increasing the system size, because excessively large-scaled jobs (in view of wall-time limit or number of resources requested) are very hard to get allocated. In addition, the labor of manually submitting multiple independent runs and managing data sets can be relieved by adopting a BigJob framework.

4.3. A Physically Unsteady Flow Field: Oscillating Boundary Problem

The accuracy of designed temporal coupling scheme is verified by solving an unsteady oscillating boundary problem. In Couette flow simulation, which converges to a steady-state flow profile, the minor inaccuracy during the flow

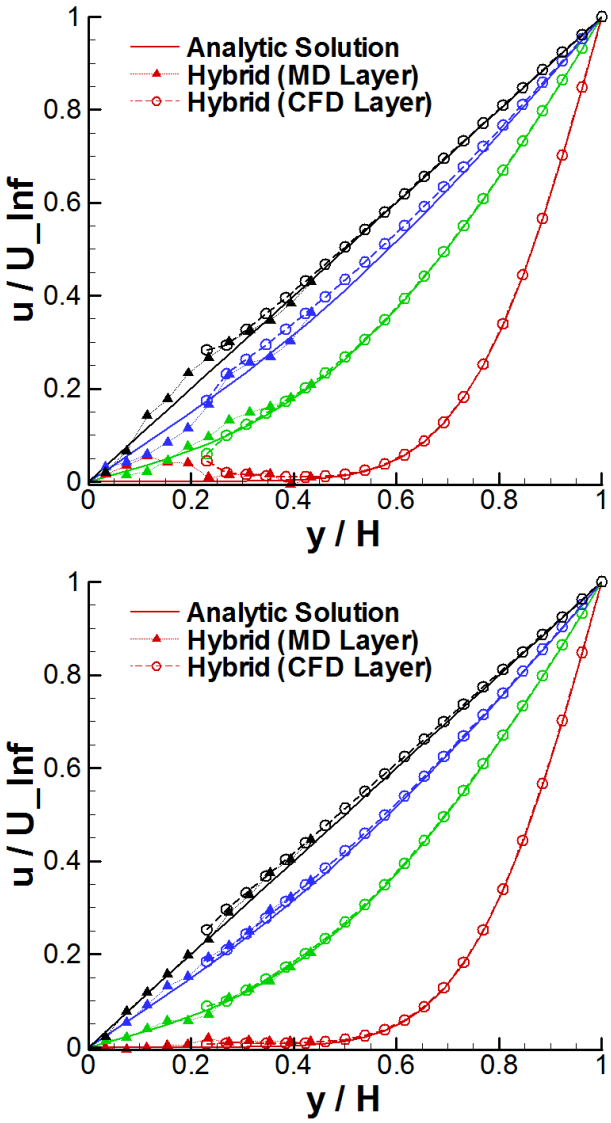

Figure 9: Couette Flow Profile with the Upper Plate Velocity of 0.25 σ/τ; The noisy solution when 4 individual simulations are averaged (left) is resolved by sampling 16 independent runs (right). Red lines denote the solution at 20 τ; Green, blue and black lines are solutions at 100, 200 and 1500 τ, respectively.

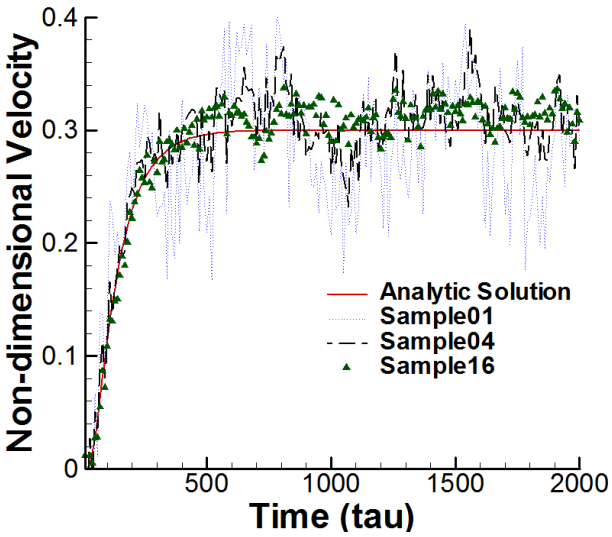

Figure 10: Variation of Continuum Velocity at the Position of 0.3 Height from the Bottom Wall (Middle of the Overlapping Region); Velocity changes at various sampling runs are compared with the analytic solution. In case 16 simulations are averaged, the noise is about 5 % compared to the analytic solution.

evolution can be eventually recovered. On the other hand, the inaccurate solution at an one instance harms the flow field afterwards in this physically unsteady problem. Therefore, the accuracy of temporal coupling scheme becomes more important. Also, velocity in the hybrid region becomes far slower than the Couette flow profile, so that the influence of noise from MD side is concerned to be more critical in the current flow simulation. The computational domain and coupling conditions are the same as the above Couette flow simulation. In this case, the upper wall boundary condition changes from the fixed velocity to oscillatory wall, which is $u_{wall}(t) = (\sigma/\tau)\times sin(2\pi t/T)$. Period T is set to be 200τ.

Figure 12 shows the oscillatory velocity profile by pure CFD and hybrid simulations. From the left figure, velocity profiles at each time instance are roughly the same between the pure CFD and hybrid simulations in magnitude. This provides that the hybrid simulation approach is also applicable to time-varying flow simulations. Meanwhile, the temporal variation of the horizontal velocity in the middle of hybrid region expresses that the noise in hybrid solution is not negligible considering the ratio between continuum and hybrid velocities. We claim that this noisy solution is caused by the

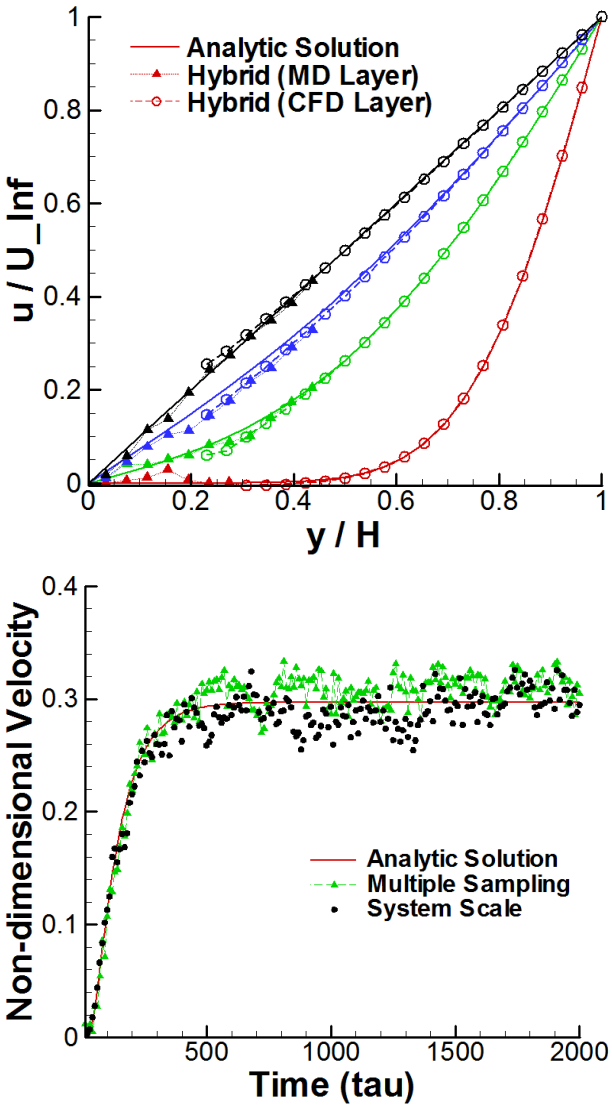

Figure 11: (Left) Couette Flow Profile in Increased System Size; Accurate flow profile can be obtained by increasing the system size 16 times larger when the velocity is reduced to 1/4. Red lines denote the solution at 20 τ; Green, blue and black lines are solutions at 100, 200 and 1500 τ, respectively. (Right) Variation of the Velocity in the Middle of Overlapping Region; Solutions by multiple sampling and increasing the system contain the similar strength of the noise in the solution, which is around 5 % of analytic velocity profile. This implies that multiple sampling approach can replace the increase of system size for solving moderate velocity flow.

combination of sampling error and inaccurate temporal coupling scheme. To clearly examine the effect of temporal coupling scheme, we sampled multiple independent experiments and compared solutions by different temporal coupling schemes.

Comparing temporal evolutions of the velocity field by different coupling schemes in Fig. 13, the clear difference is the resolution of the overshoot/undershoot phenomena by the prediction-correction approach. Sufficient numbers of independent experiments are sampled to reduce the statistical error and prediction time scale of 2.5 sampling intervals is chosen on prediction-correction approach to impose the interpolated boundary conditions on both domains. On conventional model, the maximal error is seen at peak points. This is a natural characteristics of the linear extrapolation that it fails to predict the correct values around the strong variation. This inaccuracy is resolved by using a prediction-correction approach and applying interpolated boundary condition from predicted flow properties. However, another numerical inaccuracy of time-lagging pattern in conventional model is also seen in the prediction-correction model. This necessitates the implementation of higher-order interpolation schemes.

Plots in Fig. 14 quantifies the scale of inaccuracy according to the hybrid boundary condition imposition. In the conventional model, the velocity difference ranges from -0.017 to 0.015 σ/τ. The magnitude of this error reduces as we apply the prediction-correction approach and increase the prediction time scale from 0.5 (corrected extrapolation) to 1.5 (MD interpolation) and 2.5 (both interpolation) sampling intervals. The clear difference between the conventional extrapolation model and corrected extrapolation in prediction-correction approach demonstrates that the extrapolation from two "previous" properties contains a lot more error compared to extrapolating from the current value. The similar variation between extrapolation and MD interpolation in prediction-correction approach emphasizes that the accuracy of boundary condition in CFD domain is as important as the boundary condition in MD domain. Lastly, the solution error form the conventional model is reduced by half with the imposition of interpolated boundary conditions on both domains.

5. Performance Analysis of a Multi-physics Simulation Framework

The BigJob framework is expected to save total runtime of a coupled multi-task simulation than conventional (and direct) job submissions. Logical

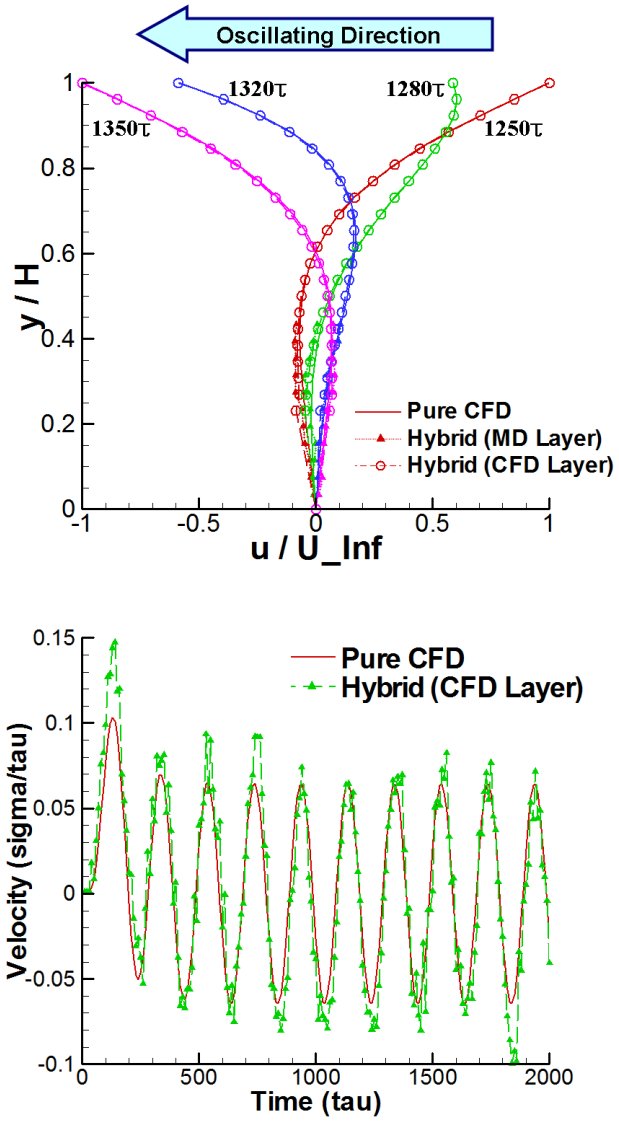

Figure 12: Unsteady Flow Profile of Stokes Boundary Layer Problem; (Left) Velocity profiles by pure CFD and hybrid simulations at specified time instances. Difference between hybrid and pure CFD solutions in hybrid region shrinks in the continuum domain. Noise from the MD simulation does not affect the global velocity profile a lot, because the driving force in this simulation is the oscillating velocity from CFD domain. (Right) Temporal variation of the velocity in the middle of hybrid layer. History of the velocity field reveals that the hybrid solution contains much noise in this experiment.

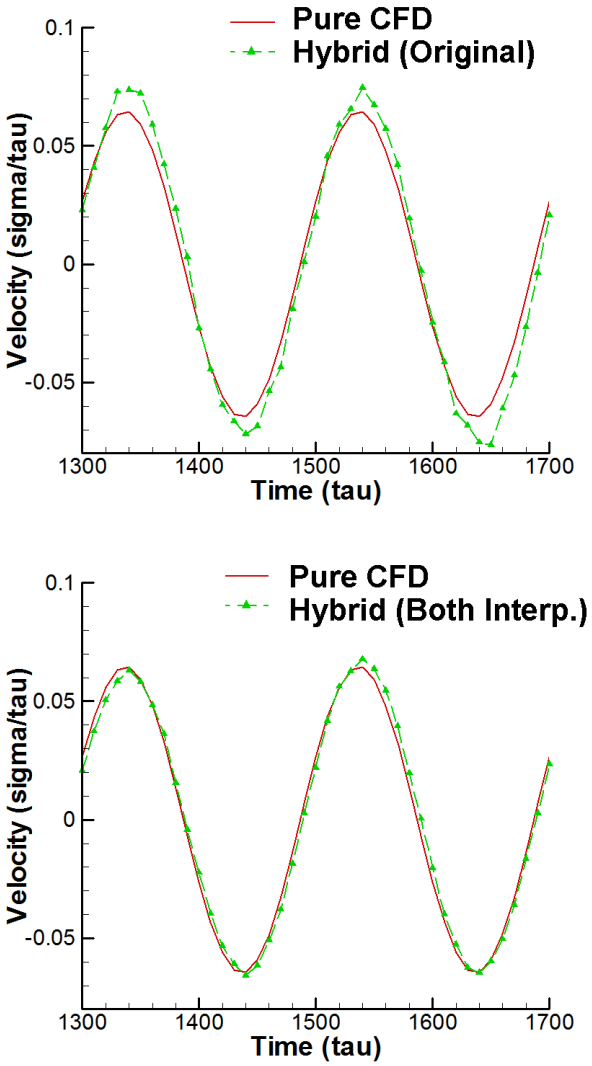

Figure 13: Temporal Variation of the Velocity in the Middle of Hybrid Layer; (Left) With conventional model, large overshoot/undershoot phenomena are observed on the peak points: the statistical noise around 0.01 σ/τ is nearly 20 % of continuum velocity. The time-lagging effect is also captured. (Right) Overshoot/undershoot phenomena in the conventional approach is almost resolved by applying the prediction-correction approach. The interpolated hybrid boundary conditions are imposed on CFD and MD domains.

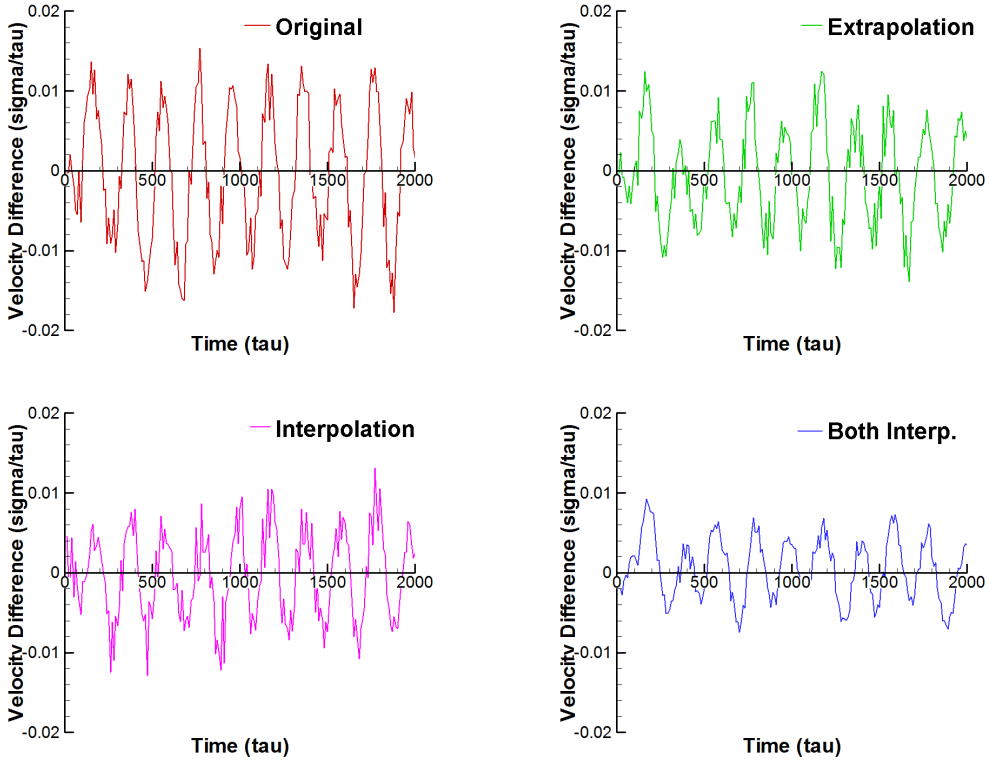

Figure 14: Reduction of Unsteady Error by Prediction-Correction Approach; Figures show the velocity difference between pure CFD and hybrid solutions in the middle of hybrid layer. Plotted data include the conventional extrapolation model and 3 different types of prediction-correction approaches, which are corrected extrapolation model, interpolated boundary model on MD domain and interpolated boundary condition on both domains. The velocity difference in the conventional model ranges from -0.017 to 0.015. This error reduces to be within -0.007 and 0.009 in refined model.

bases are as follows:

1. Many supercomputing centers adopt the queueing policy of assigning higher priority on bigger jobs. This increases the probability that a bigger-sized task gets allocated faster than the smaller one(s).
2. Independlently submitted multiple tasks are usually allocated at different physical time. So, requested wall-time limit should be sufficiently large to cover both maximal waiting time and computation time in case of coupled simulations. On the other hand, co-scheduling of coupled tasks is inherently guaranteed in a packaged job. So wall-time limit can be determined according to the actual computation time.
3. Load-balancing among multiple tasks can be dynamically achieved by changing the resource allocation to individual task during the simulation. It can be possible only when coupled yet distributed tasks are scheduled in the umbrella of a packaged job.

In this section, we present our numerical experiments to verify the above logics.

5.1. Waiting Time according to the Size and Wall-time Limit of an Individual Job

Many factors effect the waiting times, arguably the most important of them are the existing job requests on the resource at the instant of submission, requested wall-time limit and also the number of cores requested. Two other factors that effect this are the backfilling capability (which allows the running of a small job in between higher priority jobs with larger and longer resource requests) and the changes in the priority of submitted job when a particular higher priority job joins the queue. Of these factors, number of requested resources and wall-time limits are what can be handled by users and can be systematically accounted for.

We designed experiments to determine if running larger and/or longer simulations effects the actual waiting time on the queue. We submitted jobs of different sizes and different wall-time limits at the same time. Each time we submitted a job, we gathered the actual waiting time on the queue. We performed our experiments on a sufficiently large and crowded system – around i400 nodes each with 16 cores. We argue that the use of this large and crowded system increases the credibility of our experiments: it reduces the possibility of self-interference between our job submissions (i.e., our requests are allocated in a succeeding pattern). Considering the internal queueing

policy of supercomputing centers, such as credential, fairshare, resource and service priority, each user account has the restricted number of concurrent job submission and the allocation history affects the priority of next submitted job. So, we submitted different wall-time limit jobs from different user accounts in the same group allocation, and we put enough idling time between individual experiment to recover the priority of each account to the initial level. Results from 10 independent experiments are averaged for measurement.

Table 3 demonstrates the queue waiting time according to the size and wall-time limit of the job. Regarding the influence of job sizes on waiting time, jobs with larger core counts have typically lower wait times, with the exception at 128 cores which is presumably affected by the backfilling capability. Waiting time with 1000+ cores shows the stiff decrease particularly because it is granted with the higher priority in this queueing policy. The same applies to the increase of waiting time with the wall-time limit of 48, which is administrated by the different queue. The effect of wall-time limit on waiting time is not clear in our experiment, in case they are on the same queue (6- and 24-hour jobs). Collectively, submitting a BigJob for the coupled simulation instead of individually submitting multiple smaller tasks *at least* provides the comparable waiting time on the queue even when small jobs are "ideally" allocated (i.e., all jobs are allocated at the same time).

5.2. Waiting Time for a Coupled Simulation

Looking back on the scenario maps in Fig. 5, the result at Sec. 5.1 provides the waiting time between a BigJob and a first-allocated conventional job. We expect more performance gain by eliminating the inactive idling time (i.e., the difference between the waiting time of the two jobs) through the use of a BigJob.

Table 4 presents the waiting time of a BigJob with size 2X and two conventional job submissions with size X each. We experimented on two different wall-time limits (6 and 24 hours) and two different core requests (256 and 512 cores in total). A BigJob submission shows faster allocation except the small number of cores are requested for a long time, although the waiting time for the first-to-start job was smaller in the conventional job submission mode (S0) than the BigJob (S1). Interestingly, the inactive mode in conventional job submission is observed to become quite larger as the wall-time limit increases: users get to waste more allocation time as they increase wall-time limit. From the result, bigger and longer jobs tend to start faster

Table 3: Effect of Job Configurations on Waiting Time; The tables show the queue waiting times depending on the number of cores and requested wall-time limits. Measurements are made on Ranger system, which is a TeraGrid resource located at Texas Advanced Computing Center. Analyzing the actual waiting time as a function of the number of cores at different wall-time limits, it can be said that better more often than not, the waiting time decrease as the requested number of cores increases. The relationship between the waiting time and wall-time limit is harder to quantify. However, obtained numbers provide a good case study for showing the variance of actual queue waiting times. 10 independent experiments are sampled and expressed in seconds as "mean±SD".

Number of Processors	Requested Wall-time on Ranger		
	6 Hrs	24 Hrs	48 Hrs
128	24287.14±15724.91	25941.71±13878.78	44012.14±44537.75
256	27606.57±19207.95	26878.86±15108.29	67876.29±70713.95
512	27930.43±18496.98	24361.43±14849.23	32097.14±27617.86
1024	13514.57±11373.68	16372.43±10857.48	22134.71±11089.26

(comparing individual experiment), but it is hard to affirm this tendency as the general phenomenon because individual experiment has been performed at different time.

5.3. Performance Gain through Load Balancing

A BigJob framework in itself does not provide any performance gain during the simulation: a load balancer (LB) in a BigJob framework provides the better parallel performance by redistributing cores to individual sub-job within a context of packaged job. LB measures the performance of individual sub-job during the temporary stop and evolves application codes with changed number of cores. So, each code is scheduled to stop-and-restart several times for the complete simulation. It necessitates the capability of the application-level checkpointing and generic domain partitioning routine in application codes (both of which are incorporated capacities in most legacy codes).

The benefit of a LB in a BigJob framework is that it can be applied to any types of coupled applications. On the other hand, it is not highly required for the current application in two reasons: (1) in a hybrid CFD-MD simulation, MD usually requires far more computing power that most resources are dedicated to molecular dynamic simulation; (2) computational

Table 4: Waiting and inactive time for conventional job submissions, and a single BigJob submission. Average of 10 independent runs are presented in seconds. In the first two cases, conventional job is submitted to use 2×128 cores and a BigJob requests 256 cores: latter two cases use 2×256 and 512 cores, respectively. Conventional job submission mode showed faster time-to-start (i.e., waiting time of the first job + inactive mode) with 24 hr - 256 core request, and a BigJob is allocated faster in all other cases.

Number of Cores	Wall-time	Scenario	Time-to-start
256	6 Hrs	S0	20237.9 + 1045.3
		S1	19720.3
	24 Hrs	S0	5035.8 + 9933.3
		S1	16165.0
512	6 Hrs	S0	15515.7 + 446.1
		S1	15825.4
	24 Hrs	S0	4182.6 + 11096.3
		S1	13627.9

cost for the current application in Sec. 4.1 is so small that it is not necessary to endeavour to apply the load-balancing capability. This leads us to increase the computational cost of each simulation, for the purpose of evaluating the LB in a BigJob framework. In this experiment, CFD domain size is increased by 500 times and MD domain is increased by 20 times. CFD and MD codes are scheduled to have 10 simulation loops: initially start with tne same number of cores and experience nine stop-and-restarts with changed resource allocation according to the result of a LB.

Runtimes of the coupled simulation with a single BigJob is given on Table 5. In all scenarios, the same number of cores are initally assigned to CFD and MD simulations. Processors distribution in $S1_{LB}$ is changing during the simulation according to the result of a LB function. For both simulations, the time difference between S0 and S1 are within 1%. This explains that the possible overhead of a BigJob due to the communication with the advert server (for minitoring the status of sub-jobs) are negligible. In cases of load-balanced BigJob simulations, there is a significant reduction in the runtime compared to the default BigJob application when 256 cores are used – 23.1%. For larger problem set, the performance gain through the application of a LB is relatively small (7.0%), whose reason is discussed below.

The validity of a LB can be discussed from the variation of the resource

Table 5: Results of simulation runtime for S0 (conventional job submissions), S1 (default BigJob) and $S1_{LB}$ (a BigJob with load-balancing). 256 and 512 cores are used for the coupled simulation. For both cases, S0 and S1 show nearly identical computational cost because the same resource distribution is applied for the coupled simulation. With the load-balancing capability enabled, $S1_{LB}$ shows about 23.5% and 6.1% runtime save compared to S0 when 256 and 512 cores are used. All measured times are in seconds and 5 distinct experiments are averaged.

Number of Cores	Scenario		
	S0	S1	$S1_{LB}$
256	12306.0	12248.7	9413.7
512	7834.2	7910.6	7357.6

distribution between sub-jobs during the simulation. For the result of a 256 core (=16 nodes) simulation in Fig. 15, both CFD and MD sub-jobs are assigned with 8 nodes initially. From the next simulation loop, the resource distribution converges to 3 to 13 nodes between CFD and MD respectively and this ratio is maintained throughout the simulation. CFD and MD computation times change from 260 – 1235 seconds at initial loop to 705 – 850 seconds after load-balancing. Simulation runtimes are measured to be about 35 seconds longer than the slower simulation (MD simulation) per each simulation loop, which are the overhead by the initialization, I/O, and communication between coupled applications.

The result of computation time evolution in 512 cores (=32 nodes) case is presented in Fig. 16. Compared to the above experiment when smaller cores are used, the load-balancing solution shows noisier pattern. In detail, a LB fails to find the optimal solution at the first simulation loop, and the node allocation after load-balancing fluctuates between 3 – 29 and 4 – 28 nodes to each application. This is caused by two reasons. First, individual code has poor scalability. Initial simulation time for CFD and MD applications are measured around 230 and 780 seconds and the LB proposes the node distribution from 16 – 16 to 8 – 24. However, the computation time at the next simulation loop are measured to be 275 and 680 seconds, respectively. Therefore, the LB has to search for the optimal solution one more time. This is the limit of load-balancing functions which are incorporated in schedulers, since they have to manage black-box applications with unknown problem size based on restricted information. Another reason for the fluctu-

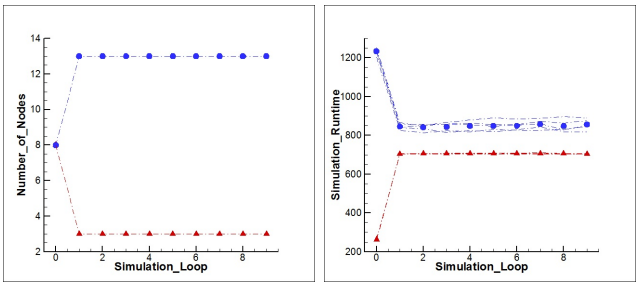

Figure 15: Change of Resource Distribution and Computation Time between CFD and MD Sub-jobs using 256 Cores (=16 Nodes); A LB detects the distribution of 3 – 13 nodes to CFD and MD sub-jobs as the optimal solution. In view of simulation runtime, 1270 seconds for the initial simulation loop reduces to 885 seconds after load-balancing is achieved. Note that each node (which contains 16 cores in the current system) is dedicated to a single application. Triangle and circle symbols denote averaged values from CFD and MD sub-jobs. Dashed lines are solutions from the individual experiment.

ation is the momentary overhead in computing system. In our experiment, MD simulation times when 28 nodes are used vary from 610 seconds to 880 seconds, depending on the magnitude of internal overhead. This evaluates the necessity of a LB as a self-correcting tool in response to the instability of a system.

Two things remained for open discussions are how to effectively measure the actual simulation time of individual sub-job and how to determine the number of simulation loops. We put time checking routines in between inter-domain communication routine and accumulate the time for running iteration loop of each code. Based on our knowledge, there is no way of systemically gathering the individual simulation time except this manual deployment. Regarding the number of simulation loops, excessive number of loops increase the I/O-related overhead (storing checkpointing solution and restarting from that); insufficient number of loops increases the simulation time at initial imbalanced configuration and degrades the capability of a LB for adapting to the unpredicted internal overhead.

6. Next Step: Further Refinement

The empirical mathematical equation on sampling noise has been presented in Sec. 4.1. We argue that this is a refined model compared to previous mathematical expressions. However, the formulation has not been verified

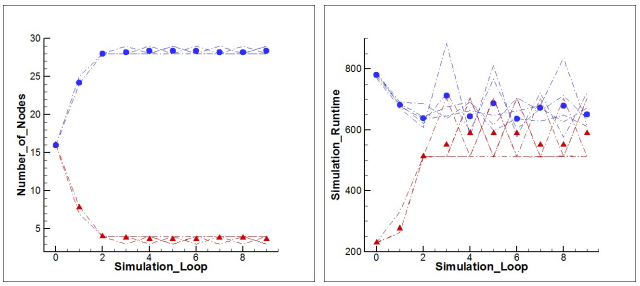

Figure 16: Change of Resource Distribution between CFD and MD Sub-jobs and Resultant Computation Time using 512 Cores (=32 Nodes); A LB solution fluctuates between 3 – 29 and 4 – 28 nodes assigned to CFD and MD sub-jobs, because of temporary internal overhead of a system. Initial simulation runtime around 815 seconds is reduced to be 725 seconds after the load-balancing is achieved, because of the poor scalability of application codes for this problem set. The same caption is used as in Fig. 15.

by various systems and conditions: coefficients will be changing according to the distance from the wall, characteristics of fluid and solid elements, etc. More rigorous research is required to address a globally acceptable equation of sampling noise.

Unsteady flow simulation in Sec. 4.3 verifies that the prediction-correction approach provides more accurate solution than conventional temporal coupling scheme. The new approach is especially powerful in resolving the unfavorable overshoot/undershoot phenomena. On the other hand, the slight time-lagging effect in the conventional model has not been improved by the prediction-correction approach. We expect that this phenomenon can be resolved by applying higher-order extrapolation/interpolation on hybrid boundary regions.

7. Conclusions

Accurate and efficient multi-scale flow simulations by a hybrid CFD-MD simulation framework have been presented in this paper. Constrained Lagrangian dynamics equations of motion and file-based hybrid interfaces are implemented on a highly-reliable LAMMPS molecular dynamics package and a verified in-house incompressible CFD code. They are virtually integrated as a single BigJob framework.

A number of numerical issues which harm the accuracy of a hybrid solution have been explored. First, quantifying the sampling noise from a

stationary flow has been proposed as a way of determining coupling parameters. We argue that our simple and intuitive idea unveils the influence of individual coupling parameter on the magnitude of statistical error and is very cost-effective in contrast to traditional trial-and-error approach. Moreover, the empirical equation derived from the stationary flow simulation describes that well-know mathematical expressions on statistical error are not accurate on nano-scale wall-bounded systems. Second, sampling multiple independent replicas has been introduced to refine the sampling noise of an individual solution and to explore to the low-speed flow regimes. This approach is superior to simulating a single large-scale problem set which is technically bound by computing capacity. The application to a Couette flow simulation in O(10) m/s velocity field is the first successful report of a moderate-speed flow simulation using a hybrid CFD-MD approach. Last, a prediction-correction approach has been designed for the accurate unsteady simulation. This approach acquires better solution by enabling the imposition of interpolated hybrid boundary conditions. The application to the oscillating boundary problem expresses that the current approach diminishes the overshoot/undershoot phenomena in the conventional methods.

Along with numerical issues, computational issues for the efficient coupled simulations have been also discussed. We introduced a BigJob framework and this directly solves the co-scheduling problem among logically separated sub-tasks. A simple load-balancing function is also implemented on a BigJob framework, to achieve the load-balancing among those separated-yet-coupled codes. From numerical experiments, we evaluate that a BigJob is very powerful in reducing the waiting time of the coupled simulation. Also, a simple load-balancing function employed in a BigJob is effective in reducing the simulation runtime.

We emphasize that above numerical investigations ease the challenge to the hybrid simulation and broaden the application area. Also, our computational experiments contribute on how to efficiently conduct coupled simulations. ***Jeff: Plz fill this last paragraph!

Acknowledgements

This work is part of the Cybertools (http://cybertools .loni.org) project and primarily funded by NSF/LEQSF (2007-10)-CyberRII-01. Important funding for SAGA has been provided by the UK EPSRC grant number GR/D0766171/1 (via OMII-UK) and HPCOPS NSF-OCI 0710874. This

work has also been made possible thanks to computer resources provided by TeraGrid TRAC TG-MCB090174 and LONI resources.

References

[1] S. T. O'Connell, P. A. Thompson, Molecular dynamics continuum hybrid computations: a tool for studying complex fuid flows, Phys. Rev. E 52 (1995) R5792–R5795.

[2] X. B. Nie, S. Y. Chen, W. N. E, M. O. Robbins, A continuum and molecular dynamics hybrid method for micro- and nano-fluid flow, J. Fluid Mech. 500 (2004) 55–64.

[3] X. Nie, S. Chen, M. O. Robbins, Hybrid continuum-atomistic simulation of singular corner flow, Phys. Fluids 16 (10) (2004) 3579–3591.

[4] J. Cui, G. W. He, D. Qi, A constrained particle dynamics for continuum-particle hybrid method in micro- and nano-fluidics, Acta. Mech. Sin. 22 (2006) 503–508.

[5] Y. C. Wang, G. He, A dynamic coupling model for hybrid atomistic-continuum computations, J. Comput. Phys. 62 (2007) 3574–3579.

[6] T. H. Yen, C. Y. Soong, P. Y. Tzeng, Hybrid molecular dynamics-continuum simulation for nano/mesoscale channel flow, Microfluid Nanofluid 3 (2007) 665–675.

[7] J. Liu, S. Chen, X. Nie, M. O. Robbins, A continuum-atomistic multi-timescale algorithm for micro/nano flows, Commun. Comp. Phys. 4 (5) (2008) 1279–1291.

[8] N. G. Hadjiconstantinou, A. T. Patera, Heterogeneous atomistic continuum representations for dense fluid systems, Comput. Phys. Commun. 4 (1997) 967–976.

[9] N. G. Hadjiconstantinou, Hybrid atomistic-continuum formulations and the moving contact-line problem, J. Comput. Phys. 154 (1999) 245–265.

[10] N. G. Hadjiconstantinou, A. L. Garcia, M. Z. Bazant, G. He, Statistical error in particle simulations of hydrodynamic phenomena, J. Comput. Phys. 187 (2003) 274–297.

[11] P. K. T. Werder, J. H. Walther, Hybrid atomistic-continuum method for the simulation of dense fluid flows, J. Comput. Phys. 205 (2005) 373–390.

[12] E. M. Kotsalis, J. H. Walter, E. Kaxiras, P. Koumoutsakos, Control algorithm for multiscale flow simulations of water, Phys. Rev. E. 79 (2009) 045701.

[13] E. G. Flekkϕy, G. Wagner, J. Feder, Hybrid model for combined particle and continuum dynamics, Europhys Lett. 52 (2000) 271–276.

[14] G. Wagner, E. G. Flekkϕy, J. Feder, T. Jossang, Coupling molecular dynamics and continuum dynamics, Comput. Phys. Commun. 147 (2002) 670–673.

[15] R. Delgado-Buscalioni, P. V. Coveney, Continuum-particle hybrid coupling for mass, momentum and energy transfers in unsteady flow, Phys. Rev. E 67 (046704) (2003) 1–13.

[16] R. Delgado-Buscalioni, P. V. Coveney, Usher: An algorithm for particle insertion in dense fluids, J. Chem. Phys. 119 (2) (2003) 978–987.

[17] R. Delgado-Buscalioni, P. V. Coveney, Hybrid molecular-continuum fluid dynamics, Phil. Trans. R. Soc. Lond. A 362 (2004) 1639–1654.

[18] G. Giupponi, G. D. Fabritiis, P. V. Covney, A hybrid method coupling fluctuating hydrodynamics and molecular dynamics for the simulation of macromolecules, J. Chem. Phys. 126 (2007) 154903–1–154903–8.

[19] S. E. Rosers, D. Kwak, An upwind differecing scheme for the time-accurate incompressible navier-stokes equations, AIAA J. 28 (1990) 253–262.

[20] S. Yoon, A. Jameson, Lower-upper symmetric-gauss-seidel method for the euler and navier-stokes equations, AIAA J. 26 (1988) 1025–1026.

[21] M. M. Rai, S. R. Chakaravarthy, An implicit form of the osher upwind scheme, AIAA J. 24 (1986) 735–743.

[22] B. V. Leer, Towards the ultimate conservative difference scheme. v. a second order sequel to godunov's methods, J. Comput. Phys. 32 (1979) 101–136.

[23] K. Travis, K. Gubbins, Poiseuille flow of lennard-jones fluids in narrow slit pores, J. Chem. Phys. 112 (2000) 1984–1994.

[24] LAMMPS. [link].
URL `http://lammps.sandia.gov`

[25] J. L. Steger, F. C. Dougherty, J. A. Benek, A chimera grid scheme, Advances in Grid Generation FED Vol. 5 (1983) 59–69.

[26] SAGA - A Simple API for Grid Applications. [link].
URL `http://saga.cct.lsu.edu/`

[27] Open Grid Forum. [link].
URL `http://www.ogf.org/`

[28] A. Luckow, S. Jha, J. Kim, A. Merzky, B. Schnor, Adaptive distributed replica-exchange simulations, Philosophical Transactions of the Royal Society A: Crossing Boundaries: Computational Science, E-Science and Global E-Infrastructure Proceedings of the UK e-Science All Hands Meeting 2008 367 (2009) 2595–2606.

[29] S.-H. Ko, C. Kim, O.-H. Rho, K. W. Cho, Load balancing for cfd applications in grid computing environment, KSAS International Journal 5 (2004) 77–87.